Simulating a superradiant laser based on a thermal atomic beam

Masterarbeit

zur Erlangung des akademischen Grades
Master of Science
(MSc)

eingereicht an der
Fakultät für Mathematik, Informatik und Physik
der Universität Innsbruck

von
Martin Fasser, BSc

Betreuer:
Univ.-Prof. Dr. Helmut Ritsch

Institut für Theoretische Physik

Innsbruck, März 2022

Abstract

In this thesis we study the coupled atom-field dynamics of a superradiant laser based on a thermal atomic beam crossing a standing wave optical resonator. In order to treat experimentally relevant system sizes we need to include a very large number of atoms which prevents the use of a full quantum model, which would require an intractably large Hilbert space. As a viable alternative, we use a so-called cumulant expansion based on expectation values of suitably chosen atomic operators for selected clusters of atoms with very similar properties. In this way we circumvent the challenge of too many equations that would arise when treating each atom individually. We assume that groups of atoms behave in a sufficiently identical way so that we can use a reduced number of equations and still obtain the essential physics correctly. Here, the kinetic temperature of the atoms is assumed high enough to describe their centre of mass classically and deterministically, meaning that the initial starting positions and the initial velocities determine their full path. In a further approximation we also neglect the cavity light forces, which the photons exert on the atoms during their passage through the cavity. The initial velocity distribution along the cavity axis is a Gaussian describing a thermal atomic cloud. As we deal with a thermal atomic beam with a fluctuating number of atoms crossing the resonator the coupled atom-field system does not reach an exact steady state, but the system variables oscillate around their average values. For a large number of atomic clusters these fluctuations are rather small and the long term solution of the equations from a first order cumulant expansion yields a quasi-steady-state. In typical parameter regimes a second order model predicts minor modifications only.

As expected, in the quasi steady state the highest photon numbers appear when the atoms have close to zero velocity along the cavity axis minimizing their Doppler width and providing for a maximal gain for steady state lasing. For hotter atoms with a wider velocity distribution, the average photon numbers decrease even to a point, where lasing stops and we find virtually no field inside the cavity. Varying the number of atoms while leaving the collective cooperativity parameter $\frac{g^2 N}{\kappa \gamma}$ fixed, results in very similar numbers of photons per atom, suggesting that the total photon number scales with N^2 as expected for superradiant lasing. When we change the number of atoms and their velocities we observe that the reduced photon number stemming from a broader velocity distribution can be compensated by simply using more atoms. As a key result we predict that instead of trying to further cool down a thermal gas with a certain particle loss, one can also get a similar amount of photons inside the cavity by just using more atoms at higher temperature. However, a broader atomic distribution can

also lead to a wider output spectrum unfavourable for clock laser applications.

Comparing models of different expansion orders, we find that the results in lowest order (mean field) and a mixed order agree quite well, as long as we include the full mixed order terms (keeping the phase terms). The reduced mixed order expansion, where one discards some phase dependent terms, however, only agrees with the mean field in certain restricted parameter regions, which do not cover our targeted regime. For experimentally relevant parameters we had to keep all equations in the full mixed order. In a final chapter we studied the effects of a velocity cut-off filter, which discards the fast fraction of the atomic distribution, on the resulting average photon number. Interestingly the absolute photon number always drops when there are less atoms in the cavity and the fast atoms thus hardly perturb lasing. Nevertheless, cutting the velocity distribution at large values lets the photon number stay at a high level for increasing temperatures. On the other hand, including the full velocity distribution the photon numbers drop quite drastically with increasing temperature.

Zusammenfassung

In der vorliegenden Arbeit untersuchen wir die gekoppelte Atom-Feld Dynamik eines superradianten Lasers, der auf einem thermischen Atom-Strahl basiert, welcher sich in einem optischen Stehwellenresonator befindet. Um experimentell relevante Systemgrößen zu behandeln, muss eine sehr große Anzahl von Atomen simuliert werden, was uns daran hindert, das volle Quanten-Modell zur Beschreibung heranzuziehen, da dessen Hilbertraum unlösbar groß ist. Als praktikable Alternative verwenden wir die sogenannte Kumulantenentwicklung, die auf Erwartungswerten von passend ausgewählten Atom-Operatoren für bestimmte Cluster von Atomen mit sehr ähnlichen Eigenschaften basiert. Dadurch umgehen wir das Problem zu vieler Gleichungen, würden wir jedes Atom einzeln behandeln. Wir nehmen an, dass sich Gruppen von Atomen ähnlich genug verhalten, sodass wir eine reduzierte Anzahl an Gleichungen benützen können, in denen trotzdem die essentielle Physik korrekt enthalten ist. Die kinetische Temperatur der Atome wird als hoch genug angenommen, sodass wir deren Schwerpunkt klassisch und deterministisch beschreiben können, also bestimmen die Anfangsbedingungen in Ort und Geschwindigkeit den gesamten Weg der Atome. Eine weitere Näherung besteht darin, die Lichtkräfte, die die Photonen während des Weges durch den Hohlraum auf die Atome ausüben, zu vernachlässigen. Die anfängliche Geschwindigkeitsverteilung entlang der Hohlraumachse ist eine Gauß-Verteilung, die eine thermische Atom-Wolke beschreibt.

Da wir einen thermischen Atom-Strahl mit fluktuierender Anzahl von Atomen, die den Resonator durchqueren, behandeln, erreicht das gekoppelte Atom-Feld System keinen stationären Zustand, sondern die Systemvariablen fluktuieren um ihren Durchschnittswert. Diese Fluktuationen sind für eine große Anzahl an Atom-Clustern eher klein und die Langzeit-Lösung der Gleichungen in erster Ordnung der Kumulantenentwicklung führt schließlich zu einem quasi-stationären Zustand. In typischen Parameterregionen sagt ein Modell 2ter Ordnung nur kleinere Änderungen voraus.

Wie erwartet erhalten wir die maximale Anzahl an Photonen im quasi-stationären Zustand, wenn die Atome entlang der Hohlraumachse eine Geschwindigkeit nahe bei null haben, was die Doppler-Breite minimiert, so ermöglichen die Atome den maximalen Gain für den Laser. Für wärmere Atome mit breiterer Geschwindigkeitsverteilung verringert sich die durchschnittliche Photonenzahl bis zu einem Punkt, an dem der Laserbetrieb stoppt und sich kein kohärentes Feld und keine Photonen mehr im Hohlraum befinden. Variieren der Atomzahl bei gleichzeitiger Fixierung der kollektiven Kooperativität $\frac{g^2 N}{\kappa \gamma}$ resultiert in sehr ähnlichen Photonenzahlen pro Atom, was darauf hindeutet, dass die

Photonenzahl mit N^2 skaliert, wie bei einem superradiantem Laser erwartet. Wenn wir die Anzahl der Atome und deren Geschwindigkeit verändern, sieht man, dass die reduzierte Anzahl an Photonen aufgrund einer breiteren Geschwindigkeitsverteilung dadurch kompensiert werden kann, dass man mehr Atome in der Verteilung nützt. Als wichtiges Ergebnis sagen wir voraus: Anstatt das thermische Gas mit weiterem Teilchenverlust weiter zu kühlen, kann man eine ähnliche Anzahl an Photonen im Hohlraum dadurch erhalten, mehr Atome bei höherer Temperatur zu verwenden. Allerdings kann eine breitere Verteilung auch zu einem breiteren Spektrum führen, was sich nachteilig auf Anwendungen der Uhren-Laser auswirken würde.

Wenn wir die Modelle verschiedener Entwicklungsordnungen vergleichen, sehen wir, dass die Ergebnisse in niedrigster Ordnung (Molekularfeldnäherung) und einer gemischten Ordnung gut miteinander übereinstimmen, zumindest solange wir die volle gemischte Ordnung verwenden (die Phasen – Terme werden nicht vernachlässigt). Die Entwicklung in reduzierter gemischter Ordnung, bei der wir manche Phasen–Terme vernachlässigen, stimmt mit der Molekularfeldnäherung nur in bestimmten Parameterregionen überein, die unsere Zielparameterregion nicht überdecken. Für diese experimentell benutzten Parameter müssen alle Gleichungen der vollen gemischten Ordnung behalten werden. In einem letzten Kapitel untersuchen wir, welchen Einfluss ein Geschwindigkeitsfilter, der den schnellen Anteil der Atome herausfiltert, auf die Anzahl der Photonen hat. Interessanterweise verringert sich die Photonenzahl immer, wenn sich weniger Atome im Hohlraum befinden und die schnellen Atome stören den Laserbetrieb kaum. Außerdem lässt ein Abschneiden der Geschwindigkeitsverteilung bei großen Werten für steigende Temperatur die Photonenzahl hoch bleiben. Wenn wir jedoch die volle Geschwindigkeitsverteilung inkludieren, fallen die Photonenzahlen ziemlich drastisch mit steigender Temperatur.

Danksagung

Als allererstes möchte ich mich bei meiner Familie bedanken, im besonderen bei meinen Eltern und bei meiner Schwester, mit denen ich eine wunderschöne Kindheit erleben durfte. Sie haben mir immer Mut gemacht und mich das ganze Studium finanziell unterstützt.

Ein besonderer Dank gilt auch der Arbeitsgruppe von Prof. Helmut Ritsch, die mich (schon bei der Bachelorarbeit) mit offenen Armen aufgenommen hat. Ganz besonders möchte ich mich bei David Plankensteiner und Christoph Hotter bedanken, die immer Zeit für meine Fragen hatten und mit neuen Ideen und Vorschlägen aufwarteten, wenn sie mir ausgegangen sind. Außerdem möchte ich mich bei Laurin Ostermann bedanken, der mir vor allem bei allen technischen Fragen eine große Hilfe war. Zum Schluss möchte ich mich noch bei Prof. Helmut Ritsch bedanken, der mir ermöglicht hat in dieser tollen Gruppe meine Masterarbeit zu schreiben und der mir mit seinen Vorschlägen immer weitergeholfen hat.

Als letztes will ich mich noch bei meinen Freunden bedanken, ohne die meine Studienzeit nicht einmal halb so schön gewesen wäre.

Contents

Chapter 1.

Introduction

In physics it is essential to measure quantities with high precision and accuracy. This allows us to determine natural constants, predict outcomes of experiments, test our theories and discover new effects when the discrepancy between prediction and experiment is too large to be explained by mere statistics. Consequently, better precision and accuracy lead to discovering new effects and therefore constitute scientific progress. Naturally, the quantities we are able to measure most precisely play a big role. With the help of lasers with small linewidths, time and frequency become such accurately measurable quantities. Atomic clocks, based on lasers, allow us to measure time with such precision, that we can test the theories of relativity and lasers in a large interferometer enable us to detect gravitational waves. Even in everyday-life lasers exert their influence: the GPS navigation system works with precise time measurement based on atomic clocks only. It is therefore no surprise that decreasing the linewidth of lasers is of high relevance and promises scientific progress.

The current main hindrance for higher precision of atomic clocks is the linewidth of the laser that operates on the ultra-narrow clock transition [1]. These lasers have to be stabilized using high-Q cavities. The cavity mirrors, however, are subject to thermal noise and therefore prevent the linewidth to go below a certain threshold. This is the main reason, why the linewidth can not be reduced further [1]. To circumvent this problem, one could directly obtain the light from an ultra-narrow atomic clock transition. While simple, the fluorescence is to weak, but a collective emission from many atoms would be sufficient to obtain a power large enough to be technologically relevant.

The fundamental work on such superradiance was done by Dicke in [2], where he had a look at the radiation of a gas in a volume smaller than the wavelength of the light. In this regime one has to include collective effects and can not treat each emitter independently anymore. This paper lead to much more work on the topic of coherent collective radiation. In 1982, Gross and Haroche summarized these results in their essay [3]. In 1993, Haake and Kolobov proposed a superradiant laser [4], where one uses this collective emission. In their model, they found the intensity to be proportional to the square of the number of atoms, while the linewidth scales inversely proportional to this. D. Meiser et al. showed in [1] that these collective emission can be achieved inside bad

cavities in 2009. In the paper [5] from 2012, Bohnet et al. proposed a superradiant laser with less than one intra-cavity photon. Such a laser would operate in the so-called "bad cavity" regime, where the spontaneous emission rate γ is much smaller than the cavity decay rate κ.

The fundamental linewidth of a laser is given by the so-called Schawlow-Townes formula $\Delta f = \frac{1}{4\pi} \frac{hf}{P_{\text{out}}} (\frac{2\gamma\kappa}{2\gamma+\kappa})^2$. In the good cavity limit $(2\gamma \gg \kappa)$ the Schawlow-Townes formula simplifies to $\Delta f = \frac{\kappa}{4\pi} \frac{hf}{P_{\text{out}}}$, while in the bad cavity limit $(2\gamma \ll \kappa)$ we obtain $\Delta f = \frac{\gamma}{\pi\kappa} \frac{hf}{P_{\text{out}}}$ for the fundamental linewidth. Moreover, in the bad cavity limit, the so-called frequency pulling coefficient $\frac{df}{df_{\text{cav}}} = \frac{2\gamma}{2\gamma+\kappa}$ is much smaller, so the influence of the noise in the cavity frequency is drastically reduced [5]. When operating in such a regime the collective excitation is stored in the gain medium, and therefore the atoms are mainly responsible for carrying the phase information. The authors demonstrate in [5] a superradiant laser source, in which synchronization of atomic dipoles can be sustained by very few photons inside the cavity and claim, that the linewidth of the emitted light is more than ten thousand times less than the quantum linewidth limit that one typically uses for good cavity optical lasers. For a practical implementation in 2020 Haonan Liu et al. proposed a "rugged mHz-linewidth superradiant laser driven by a hot atomic beam" [6]. The setup they considered consists of a beam of thermal atoms, that are pumped before they enter a cavity and serve as a gain medium for a superradiant laser. Along the cavity axis the velocity distribution is a thermal Maxwell-Boltzmann distribution. They demonstrated, that this kind of setup is competitive with the best clock lasers. An advantage of the proposed setup is its ruggedness, meaning it can be operated in challenging real-world environments such as improved GPS satellites, deep space navigation and new geophysical technologies.

In the following thesis we study superradiant lasing based on a thermal atomic beam. Contrary to the setup in [6], the atoms are moving in the cavity from the beginning with the same velocity distribution along the cavity axis. We start by introducing the basic concepts of a laser in the next chapter and derive important formulas, which govern the dynamics of such a system. Thereafter, we adapt these formulas to our specific model and arrive at the master equation for our system. To handle the very large number of atoms, we use a cumulant expansion to first order (mean field) and also to mixed order, which yields large sets of differential equations that we solve numerically. We study the general time evolution and the photon numbers in quasi-steady-state depending on the temperature. Furthermore, we examine the difference of reduced mixed order (where we discard the phase terms) to the full mixed order for different parameter regions. Finally, we have a look at the influence of a velocity filter for the atoms on the photon numbers. In this thesis we will mostly focus on the photon numbers. For a laser also the linewdith is very interesting. To calculate the linewidth, the approach of the so called imaginary filter cavities could be useful. This method has been introduced in [7] and successfully used for example in [8].

Chapter 2.

Basic Concepts

In this chapter we introduce the basic concepts and formulas governing the time evolution of our system. We start with a general introduction to the concept of a laser and its underlying physical mechanisms. The second section will cover the dynamics of the atoms, the field inside the cavity and their interaction, while in the third section we will introduce the Master equation as a way of dealing with open quantum systems. In the fourth section we present the cumulant expansion method in order to deal with a large number of atoms. so that we obtain a set of differential equations for operator expectation values instead of solving the full, high-dimensional Master equation.

2.1. Laser theory

In this section we will introduce the basic principles of a laser system. The laser is, in contrast to a black body radiator, a source of monochromatic and coherent light. Two crucial phenomena required to build a laser are spontaneous and stimulated emission of photons, as the acronym "**L**ight **A**mplification by **S**timulated **E**mission of **R**adiation" suggests. These two processes are depicted in figure 2.1.

On the left we depict a two-level-atom with excited state $|e\rangle$ and ground state $|g\rangle$. If the electron e^- is initially in the excited state $|e\rangle$ the atom can decay into a the ground state of lower energy. Energy conservation is still satisfied, as the excess energy is now carried away in form of a photon (symbolized by the red wavy line) with a certain frequency corresponding to the energy difference between excited and ground state. This process is called spontaneous emission, as there is no certain time at which the atom decays, rather the probability of being in the excited state decreases exponentially. The emitted photon can now encounter another two-level-atom in the excited state and initiate the so-called stimulated emission: Instead of the two-level-atom decaying spontaneously, the incoming photon stimulates the decay and therefore the emission of another identical photon with the same frequency, propagation direction, phase and polarization. These two photons can stimulate further emission from further two-level-atoms, which again amplifies the photon number and so on, resulting in an avalanche of coherent photons with all the same frequency, phase and polarization (depicted on the right in figure 2.1). To obtain a reasonably large photon number, one puts the atoms into
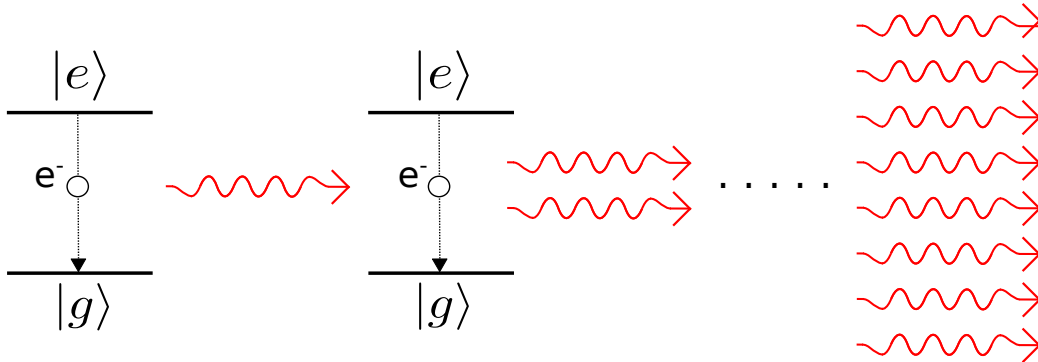
Figure 2.1.: *Basic concept of a laser.* An atom spontaneously decays, emitting a photon (red wavy arrow). This photon triggers another atom's stimulated emission of a second photon. The photons now have the same frequency, propagation direction and phase. More and more photons are created by stimulated emission, resulting in an avalanche of photons.

a cavity. The mirrors of the cavity reflect the photons back and the avalanche continues to grow. One of the mirrors is partially transmissive in order to get a laser output. If the photons encounter atoms in the ground state, they can get absorbed. Consequently, for the photon avalanche to grow instead of being diminished by absorption, we need the ensemble of atoms to be inverted, meaning that more atoms are in the excited state than in the ground state. This is, however, not possible in thermal equilibrium, which can be seen from the so-called Einstein coefficients and the phenomenological Einstein rate equations.

Suppose we have N two-level-atoms, with N_e of them in the excited state and N_g in the ground state, such that $N = N_e + N_g$. The coefficient A denotes the rate of spontaneous decay from the excited state into the ground state, and B represents the rate of absorption and stimulated emission per energy density. The rate of absorption is the same as the rate of stimulated emission, if the degeneracy of the levels is the same, which can be seen by further considerations (more details in [9]). Moreover, these rates depend on the energy density U, which is assumed to be constant. The rate of change of the ground state population $\frac{dN_g}{dt}$ now consists of three processes: the decrease due to absorption with rate $BU \cdot N_g$ and the increase due to the spontaneous decay with rate $A \cdot N_e$ and due to stimulated emission with rate $BU \cdot N_e$. As $N = N_e + N_g$ is a conserved quantity, we also have that any increase/decrease of N_g is equivalent to a decrease/increase of N_e. Altogether we arrive at

$$\frac{dN_g}{dt} = -\frac{dN_e}{dt} = A \cdot N_e + BU \cdot N_e - BU \cdot N_g \tag{2.1}$$

If we do not drive the system in any way, the energy density U is zero, the only occurring process is spontaneous emission and we arrive at the differential equation for

an exponential decay of the population in the excited level, just as discussed above. When driving the system for a long time, we will end up in a steady-state, where there is no population change anymore and we set $\frac{dN_g}{dt} = 0$. Using $N_g = N - N_e$, we rearrange equation 2.1 and find for the fraction of atoms in the excited state

$$\frac{N_e}{N} = \frac{1}{2 + \frac{A}{BU}}. \tag{2.2}$$

As A and BU are both rates, they are positive, meaning that even for very high energy densities (U approaching infinity) the fraction of atoms in the excited state will stay below $1/2$ and we therefore have no population inversion. To circumvent this problem, we will later (in section 2.4.1) discuss how to achieve population inversion. To this end, we assume, that the atoms have an auxiliary level, which we can adiabatically eliminate.

2.2. The atom and the cavity field

Let us first have a look at the description of the atom and the cavity field. To make our life simpler, we approximate all atoms as a two-level-system (TLS) consisting of a ground state $|g\rangle$ and an excited state $|e\rangle$. The levels are separated by an energy difference corresponding to the atomic transition frequency ω_a, which lies close to the cavity resonance frequency ω_c. The difference between these two frequencies is called the detuning $\Delta = \omega_c - \omega_a$. As all processes are close to this transition, all other transitions are off-resonant and we can neglect the AC-Stark Shifts that would arise from treating the off-resonant transitions perturbatively. This TLS is mathematically equivalent to a spin-1/2-system. Therefore we can use the terminology developed for the spin-1/2-system, in particular we make use of the Pauli matrices. The Hamiltonian of the TLS now becomes $H_{atom} = \frac{\hbar\omega_a}{2}\sigma^z$. It is important to note, that we can add a constant term of Energy E_0 without changing the dynamics, as this will only change the global phase of the resulting wave function which will drop out anyway after calculating expectation values. We will make use of this gauge freedom later.

Next, we want to describe the quantized fields inside the cavity. The energy of the electromagnetic fields is given by

$$E = \frac{1}{2} \int dV [\epsilon_0 \mathbf{E}^2(\mathbf{r}, t) + \frac{1}{\mu_0} \mathbf{B}^2(\mathbf{r}, t)] \tag{2.3}$$

Using the source-free Maxwell equations to derive the wave equations for $\mathbf{E}(\mathbf{r}, t)$ and $\mathbf{E}(\mathbf{r}, t)$, one can verify that [10]

$$\mathbf{E}(\mathbf{r}, t) = E_0 \, q(t) \, \sin(kx) \, \mathbf{e}_y \tag{2.4}$$

$$\mathbf{B}(\mathbf{r}, t) = \frac{\mu_0 \epsilon_0}{k} \, E_0 \, q(t) \, \cos(kx) \, \mathbf{e}_z \tag{2.5}$$

satisfy the wave equation and also the boundary conditions, namely the electric field being zero at the cavity mirrors, by choosing appropriate values for k. Inserting these expressions into equation 2.3 one arrives, by fixing $E_0 = \sqrt{\frac{2\omega_c}{\epsilon_0 V}}$, at the energy of the well-known harmonic oscillator with unit mass

$$E = \frac{p^2}{2} + \frac{1}{2}\omega_c^2 q^2, \tag{2.6}$$

which we know how to quantize: Replacing the canonical variables p and q by their respective operators $\hat{p}$ and $\hat{q}$ (canonical quantization) and defining new operators by $\hat{a} = (2\hbar\omega_c)^{-1/2}(\omega_c \hat{q} + i\hat{p})$ and $\hat{a} = (2\hbar\omega_c)^{-1/2}(\omega_c \hat{q} - i\hat{p})$, one finds the Hamiltonian of the cavity field to be

$$\hat{H}_{\text{cavity}} = \hbar\omega_c\, \hat{a}^\dagger \hat{a} \tag{2.7}$$

where we have dropped the ground state energy $\frac{1}{2}\hbar\omega_c$. From the canonical commutation relation $[\hat{q}, \hat{p}] = i\hbar$ we find $[\hat{a}, \hat{a}^\dagger] = 1$. From this commutator together with equation 2.7 we see that $\hat{a}$ and $\hat{a}^\dagger$ are ladder operators, leading us to defining the Fock-states $|n\rangle$ with eigenvalue $n \in \mathbb{N}_0 = \{0, 1, 2, 3, ...\}$ as basis states for the cavity field :

$$\hat{H}|n\rangle = n\,\hbar\omega_c \tag{2.8}$$
$$\hat{a}^\dagger|n\rangle = \sqrt{n+1}\,|n+1\rangle \tag{2.9}$$
$$\hat{a}|n\rangle = \sqrt{n}\,|n-1\rangle. \tag{2.10}$$

Now that we have seen how to describe the atoms and the field by themselves, we go on to finding a description of their interaction. Classically, their interaction energy is given by $-\mathbf{d}\mathbf{E}(\mathbf{r}, t)$. In the usual experiments the wavelength is much larger than the atoms, allowing us to approximate the electric field strength being constant over the extent of an atom. Using this so-called electric dipole approximation [11] and the operator expression for the electric field 2.4, we only have to find the operator expression for the dipole moment $\mathbf{d}$. By symmetry arguments, the diagonal elements of the dipole operator vanish. Furthermore, we can choose the off-diagonal elements to be real by choosing an appropriate phase in the wave function for the ground or excited state. Therefore, we can write the dipole operator as $\hat{d} = d\,(\sigma^+ + \sigma^-)$. For later convenience, we introduce the notation $\sigma^{ij} = |i\rangle\langle j|$. We can express the Pauli-matrices as follows: $\sigma^- = \sigma^{ge}$, $\sigma^+ = \sigma^{eg}$ and $\sigma^z = \sigma^{ee} - \sigma^{gg}$. We also note, that $\sigma^{ij}\sigma^{kl} = \sigma^{il}\delta_{jk}$, which will be used later for simplifying some equations. Together with equation 2.4 we arrive at

$$\hat{H}_{\text{int}} = -\hat{\mathbf{d}}\,\hat{\mathbf{E}} = \hbar g f(x)(\sigma^{eg} + \sigma^{ge})(\hat{a} + \hat{a}^\dagger) \tag{2.11}$$

where $f(x) = \sin(kx)$ is a mode function. Multiplying out the brackets and calculating

the time evolution of the resulting operators in the Heisenberg picture yields

$$\sigma^{\mathrm{eg}}\hat{a} \sim e^{i(\omega_a - \omega_c)t} \tag{2.12}$$

$$\sigma^{\mathrm{eg}}\hat{a}^\dagger \sim e^{i(\omega_a + \omega_c)t} \tag{2.13}$$

$$\sigma^{\mathrm{ge}}\hat{a} \sim e^{-i(\omega_a + \omega_c)t} \tag{2.14}$$

$$\sigma^{\mathrm{ge}}\hat{a}^\dagger \sim e^{-i(\omega_a - \omega_c)t}. \tag{2.15}$$

As we will choose $\omega_a \approx \omega_c$, only the first and the last term are near-resonant, while the other fast oscillating terms are off-resonant. Treating the off-resonant terms with time-dependent perturbation theory, the large terms in the exponents appear in the denominator [10], making the resulting terms very small, such that we can neglect them. This approximation is known as the Rotating Wave Approximation (RWA). Putting all the previous results together, we arrive at the Hamiltonian describing an atom interacting with a cavity field mode

$$\hat{H} = \hat{H}_{\mathrm{atom}} + \hat{H}_{\mathrm{cavity}} + \hat{H}_{\mathrm{int}} = \hbar\omega_a \sigma^{\mathrm{ee}} + \hbar\omega_c \hat{a}^\dagger \hat{a} + \hbar g f(x)\left(\sigma^{\mathrm{eg}}\hat{a} + \sigma^{\mathrm{ge}}\hat{a}^\dagger\right) \tag{2.16}$$

This Hamiltonian is the well-known Jaynes-Cummings-Hamiltonian [11]. A central part of our model discussed later is based on the atoms moving in the cavity, the mode function modifies their interaction strength with the photons. This Hamiltonian is also easily extended to multiple noninteracting atoms

$$\hat{H} = \hbar\omega_a \sum_m \sigma_m^{\mathrm{ee}} + \hbar\omega_c \hat{a}^\dagger \hat{a} + \hbar g \sum_m f(x_m)\left(\sigma_m^{\mathrm{eg}}\hat{a} + \sigma_m^{\mathrm{ge}}\hat{a}^\dagger\right). \tag{2.17}$$

where $\sigma_m^\pm$ are the operators of atom m and we sum over all atoms. This Hamiltonian is the so-called Tavis-Cummings Hamiltonian [12].

2.3. Transforming into a rotating frame

From classical mechanics we know that it is sometimes convenient to switch to a certain reference frame, which can lead to a simplification of the equations of motion. The quantum mechanical analog is introduced in the following. In quantum mechanics, a general way of associating two sets of basis states with each other is a (time dependent) unitary transformation $R(t)$, such that [13]

$$|\Phi\rangle = R(t)|\Psi\rangle. \tag{2.18}$$

Assuming that $|\Psi\rangle$ satisfies the Schrödinger equation $i\hbar|\dot{\Psi}\rangle = H|\Psi\rangle$ with some Hamiltonian H, one can derive a differential equation for $|\Phi\rangle$. Using the product rule and the unitarity of the transformation $R^{-1}(t) = R^\dagger(t)$, one arrives at a transformed Schrödinger equation $i\hbar|\dot{\Phi}\rangle = \tilde{H}|\Phi\rangle$ with

$$\tilde{H} = i\hbar\dot{R}(t)R^\dagger(t) + R(t)HR^\dagger(t). \tag{2.19}$$

Choosing $R(t) = \mathbb{1}$ one trivially obtains the Schrödinger equation, from which we started. Choosing the transformation being the exponential of the full Hamiltonian $R(t) = \exp(iHt/\hbar)$ yields the Heisenberg picture. In our case we split the Tavis-Cummings Hamiltonian into two parts $H_0 + V$,

$$H_0 = \hbar\omega_{\mathrm{a}} \sum_m \sigma_m^{\mathrm{ee}} + \hbar\omega_{\mathrm{a}}\hat{a}^\dagger\hat{a} \tag{2.20}$$

$$V = \hbar(\underbrace{\omega_{\mathrm{c}} - \omega_{\mathrm{a}}}_{:=\Delta})\hat{a}^\dagger\hat{a} + \hbar g \sum_m f(x_m) \left(\sigma_m^{\mathrm{eg}}\hat{a} + \sigma_m^{\mathrm{ge}}\hat{a}^\dagger\right) \tag{2.21}$$

and choose $R(t) = \exp(iH_0t/\hbar)$ [13], which is known as the interaction picture with respect to H_0. Using the explicit expression for $R(t)$ and the well known Hadamard-Lemma $\exp(X)Y\exp(-X) = \sum_{k=0}^{\infty} \frac{1}{k!}[X,Y]_n$ with $[X,Y]_n = [X,[X,Y]_{n-1}]$ and $[X,Y]_0 = Y$, we derive an expression for the transformed Hamiltonian $\tilde{H}$ according to equation 2.19 and end up with

$$\tilde{H} = \hbar\Delta\hat{a}^\dagger\hat{a} + \hbar g \sum_m f(x_m) \left(\sigma_m^{\mathrm{eg}}\hat{a} + \sigma_m^{\mathrm{ge}}\hat{a}^\dagger\right) \tag{2.22}$$

2.4. Open Quantum Systems - the Master Equation

In physics, we are used to looking at isolated systems, which are ideal and reasonably easy to describe. However, in reality, these systems always interact with their environment. In some systems this interaction can be negligible, such that the system is sufficiently well approximated as an isolated system. In the case of a laser, though, we need these interactions to describe the laser light emerging from the cavity where we can use it for further applications. The atoms interacting with the surrounding field modes lead to spontaneous emission of a photon and de-excitation of the atoms. Moreover, the photons inside the cavity interact with the infinite modes of the vacuum field outside of the cavity, which leads to photons travelling through the cavity mirrors and being lost for the cavity dynamics. Solving the full schrödinger equation for the coupled setup of system and environment may be too hard or not necessary, if we are only interested in the evolution of the system itself, and this equation is called the "Master Equation". The case of a cavity interacting with a (thermal) environment ist studied in [9], Here, we will only give a brief overview.

The system of interest is a harmonic oscillator with hamiltonian $H_{\mathrm{sys}} = \hbar\omega a^\dagger a$ and the environment consists of multiple modes $H_{\mathrm{env}} = \sum_j \hbar\omega_j b_j^\dagger b_j$. After a rotating wave approximation, the interaction between them reads $H_{\mathrm{int}} = \sum_j g_j(a^\dagger b_j + ab_j^\dagger)$. The whole system behaves according to the equivalent of the Schrödinger equation when working with density matrices, the von Neumann equation,

$$\dot{\rho}_{\mathrm{AB}} = -\frac{i}{\hbar}[H_{\mathrm{AB}}, \rho_{\mathrm{AB}}] \tag{2.23}$$

where the index AB indicates, that the hamiltonian and the density matrix are that of the setup including system A and environment B. The idea now is to trace over the environment B and obtain an equation solely for system A. It is convenient to work in the interaction picture with respect to the bare hamiltonians of system and environment without the interaction between them. Formal integration of the von Neumann equation and substituting back into the von Neumann equation in interaction representation yields [9]

$$\dot{\tilde{\rho}}_{\mathrm{AB}}(t) = \frac{1}{i\hbar}[\tilde{H}_1, \tilde{\rho}_{\mathrm{AB}}(0)] - \frac{1}{\hbar^2} \int_0^t [\tilde{H}_1(t), [\tilde{H}_1(t'), \tilde{\rho}_{\mathrm{AB}}(t')]]\mathrm{d}t'. \tag{2.24}$$

Tracing over the environment B, the first commutator is assumed to vanish (this is true, if there is no correlation between system A and environment B at time $t = 0$), so that we only have to evaluate the partial trace of the double commutator. In order to evaluate the double commutator, we also assume that the state of the environment is not changed by the interaction with the system, and we can write $\rho_{\mathrm{AB}}(t) = \rho_{\mathrm{A}}(t) \otimes \rho_{\mathrm{B}}(0)$, which is known as the Born-Markov approximation [9]. In particular, we also neglect the influence of the history of the system: In principle, the state of the environment depends on the history of the system, and this dependence would also have an effect back on the system itself. By making the Markovian assumption, we consider the environment much larger than our system, so that the influence of the system on the environment is negligible and there is no back action of the system on itself.

In [9] the authors derive the master equation of a harmonic oscillator interacting with a thermal environment. To this end, the environment $\rho_{\mathrm{B}}(0)$ is in a coherent state with a thermal distribution of photons. As we simulate an optical cavity, we can neglect the thermal photons on the outside, which is equivalent to setting the temperature to $T = 0$. Then, we finally arrive at the following differential equation for the density operator of the system ρ_{A},

$$\dot{\tilde{\rho}}_{\mathrm{A}} = \frac{\kappa}{2}(2a\tilde{\rho}_{\mathrm{A}}(t)a^\dagger - a^\dagger a\tilde{\rho}_{\mathrm{A}}(t) - \tilde{\rho}_{\mathrm{A}}(t)a^\dagger a), \tag{2.25}$$

where κ is the photon loss rate, as we will see later. The right-hand-side of this equation is said to be of Lindblad form. In fact, a lot of interactions can be described by such a term in Lindblad form. One just has to identify the corresponding jump operator c (in our case a) and the rate Γ, at which these jumps occur (in our case κ). The general form of these Lindblad terms then looks like

$$\mathcal{L}_\Gamma \rho = \frac{\Gamma}{2}(2c\rho c^\dagger - c^\dagger c\rho - \rho c^\dagger c). \tag{2.26}$$

If we want to describe more than one interaction, we add all the corresponding Lindblad terms to the right hand side of the von Neumann equation and we call it master equation from that point on. In our model we will have three Lindblad terms of

different type: describing the spontaneous emission of the atoms, accounting for the cavity loss and we can also model the driving of the laser as such a term in Lindblad form. With methods that we will introduce in the next section, we can derive a differential equation for the operator $\langle c^\dagger c \rangle$. Starting from $\dot\rho = \mathcal{L}_\Gamma \rho$, one arrives at a differential equation of an exponential decay with rate Γ, which is also the inverse of the mean life time,

$$\langle \dot{c^\dagger c} \rangle = -\Gamma \langle c^\dagger c \rangle. \tag{2.27}$$

If we now specify c to being the atomic jump operator, then $\langle c^\dagger c \rangle$ becomes the population of the excited state, decaying with Γ, which corresponds to the spontaneous emission rate, and we can immediately associate the Γ in the Lindblad term with a physically measureable quantity, namely the spontaneous emission rate. The decay of a field inside a cavity is very similar: Specifying c to being the bosonic annihilation operator, $\langle c^\dagger c \rangle$ becomes the number of photons (and therefore also the energy). This leads us to identifying Γ with the decay rate of the cavity photon number/energy in this particular example.

2.4.1. Modeling the driving of the laser

For a system to work as a laser we need population inversion, meaning there should be more atoms in the excited state than in the ground state, as discussed in section 2.1. Such a population inversion cannot be achieved in thermal equilibrium, which can be seen from the Boltzmann factor. Moreover, coherently driving the atoms with another laser will result in Rabi oscillations, and the population will oscillate between ground and the excited state. However, even for a perfectly resonant drive we will only arrive at an average of half of the population in the excited state. Taking into account the spontaneous emission of the atoms will result in damped Rabi oscillations, therefore dropping to even below half of the population being excited. So, in order to achieve population inversion we employ a third level, the so-called auxiliary level $|a\rangle$, which energetically lies above the ground state as well as above the excited state. We pump the transition between the ground state $|g\rangle$ and the auxiliary level $|a\rangle$ with a pump laser or some other broadband sources of light. This pumping will transfer the population between the ground state and the auxiliary level. The key trick now is that there is also a decay channel from the auxiliary level $|a\rangle$ to the excited state $|e\rangle$ featuring a very large decay rate. So the atoms, initially in the ground state $|g\rangle$, are pumped into the auxiliary level $|a\rangle$, but, instead of going back to the ground state, which would result in Rabi oscillations, the atoms almost immediately decay to the excited state. In order for this to happen, the rate of decay must be much larger than the Rabi-frequency. Effectively, we have now transferred the atoms from the ground state $|g\rangle$ to the excited state $|e\rangle$. The rate of this transfer is associated with the Rabi frequency, as an atom in the auxiliary level almost immediately decays to the excited state. Adiabatic elimination of the auxiliary level $|a\rangle$ leaves us with an effective two-level-system with "spontaneous

excitation". This spontaneous excitation combines the pumping to the auxiliary level and the fast decay to the excited level to a single (incoherent) process and is the opposite of spontaneous emission, hence the name "spontaneous excitation".
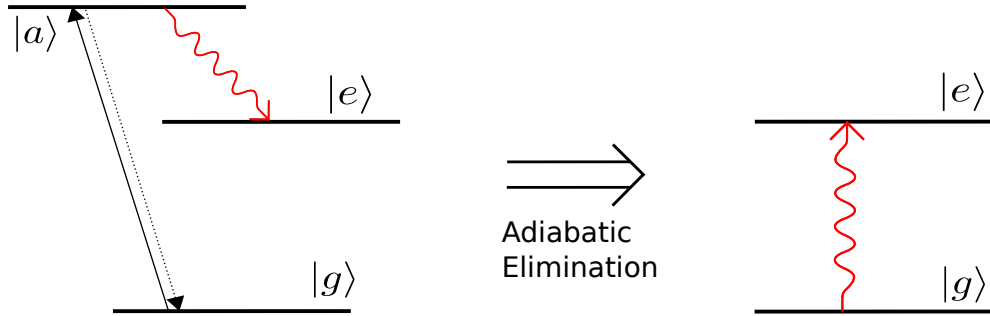
Figure 2.2.: *Sketch of the incoherent pump.* The black arrows indicate coherent transfer. But instead of getting back into the ground state (black dotted arrow), the electrons immediately decay into the excited state (red wavy line). By adiabatic elimination, we can describe these processes as depicted on the right.

2.5. Cumulant expansion

If we want to solve the Schrödinger equation for more than a few individual two-level atoms, we quickly run into a problem: if N is the number of individual atoms, the dimension of the Hilbert space scales exponentially as 2^N (for two-level-atoms), which means that for as little as $N=20$ atoms we already have 10^6 dimensions in the Hilbert space and approximately 10^{12} entries in the time evolution operator represented as a matrix. Yet, in this thesis,, we want to simulate hundreds of thousands of atoms. Solving these high-dimensional differential equations numerically takes far to much computational time, such that we have to come up with alternative methods to study the dynamics. We could investigate the dynamics in the Heisenberg picture, but there we obtain differential equations for the operators in our system, which are hard to solve. The crucial simplification, however, is performed by simulating the dynamics of the expectation values of the operators only. In the end, we want to find the expectation values of certain operators anyway. Making use of the Schrödinger picture (as the operators themselves are time independent), for a general operator $\hat{O}$ we find

$$\frac{\mathrm{d}}{\mathrm{d}t}\langle\hat{O}\rangle = \frac{\mathrm{d}}{\mathrm{d}t}\mathrm{Tr}\{\hat{O}\rho\} = \mathrm{Tr}\{\hat{O}\frac{\mathrm{d}}{\mathrm{d}t}\rho\}, \tag{2.28}$$

where we can insert the master equation for $\frac{\mathrm{d}}{\mathrm{d}t}\rho$. Using the invariance of the trace under cyclic permutation we can simplify the equations to terms including expectation values

of other operators or products of operators. In order to obtain a closed set of differential equations, we need to derive the equations for these other operators or products of operators. This could again lead to new products of operators and so on. For simple systems, e.g. a cavity with a lossy mirror described by the Master equation we have

$$\dot{\rho} = -i[\omega a^\dagger a, \rho] + \frac{\kappa}{2}(2a\rho a^\dagger - a^\dagger a \rho - \rho a^\dagger a) \tag{2.29}$$

and the set of equations closes without much effort. In fact, after deriving the equation for the photon number $\hat{O} = a^\dagger a$ we are already done, as on the right-hand-side of the equation only the expectation value of the photon number itself appears,

$$\langle \dot{a^\dagger a} \rangle = -\kappa \langle a^\dagger a \rangle. \tag{2.30}$$

However, for more complicated systems (e.g. featuring a larger number of atoms to arrive at our laser system), we will have to derive more and more equations for longer and longer products of operators. This means that we have to truncate this expansion in order to close the set. This can be done by approximating higher-order expectation values by products of lower-order expectation values. The general way of doing this was introduced by R. Kubo in [14]. A less mathematical approach is given by N. G. van Kampen in [15] and [16]. For our purpose a useful summary of the important results is given in [17]. The joint cumulant $\langle \cdot \rangle_c$ can be thought of being a measure of the correlation of the operators and can be expressed by

$$\langle X_1 X_2 ... X_n \rangle_c := \sum_{p \in P(I)} (|p| - 1)!(-1)^{|p|-1} \prod_{B \in p} \langle \prod_{i \in B} X_i \rangle \tag{2.31}$$

where $X_1, X_2, ..., X_n$ are the operators, $P(I)$ is the set of all partitions, $|p|$ is the length of the partition p and B runs over the blocks of each partition [17]. The idea here is to assume that the joint cumulant of the operators is zero. This is mathematically rigorous in the case, that two of the operators are statistically independent of each other only [14]. Here, we approximate the joint cumulant as zero, which allows us to rearrange equation 2.31 to

$$\langle X_1 X_2 ... X_n \rangle = \sum_{p \in P(I) \setminus I} (|p| - 1)!(-1)^{|p|} \prod_{B \in p} \langle \prod_{i \in B} X_i \rangle. \tag{2.32}$$

With this we are able to express higher-order expectation values in terms of lower-order expectation values, assuming, that the joint cumulant is zero. In our work we will frequently need the formula for $n = 2$ and $n = 3$, so it makes sense to write down these specific cases as

$$\langle ab \rangle \approx \langle a \rangle \langle b \rangle \tag{2.33}$$

$$\langle abc \rangle \approx \langle ab \rangle \langle c \rangle + \langle ac \rangle \langle b \rangle + \langle cb \rangle \langle a \rangle - 2\langle a \rangle \langle b \rangle \langle c \rangle \tag{2.34}$$

We see that in the case $n = 2$, one just writes the product of the expectation values instead of the expectation value of the operators' product, while it is more complicated for $n = 3$. Altogether, we are able to express expectation values of higher-order operator products by expectation values of lower-order operator products, which eventually allows us to close the set of differential equations.

Chapter 3.

The Model

After having introduced the basic concepts in the previous chapter let us now find the equations that govern the dynamics of our specific laser model.

We consider an ensemble of incoherently pumped two-level-atoms inside a lossy cavity as depicted in figure 3.1. The cavity mirrors are not completely reflective and allow for photons to leak out of the cavity with a rate κ. An incoherent pump (see section 2.4.1) is included, such that we are able to achieve population inversion. In an experiment, the atoms would be distributed over many periods of the mode function. To mimic such an experimental situation, in our simulations we distribute the atoms equidistantly along one spatial period of the resonant mode function. Moreover, we allow the atoms to move along the cavity axis. Here, we treat their movement deterministically and classically. This means that we neglect the light forces the photons exert on the atoms during absorption and emission. For this reason we only need to assign an initial velocity and position to each atom, and because of the lack of forces the velocity will stay the same throughout the entire simulation. Together with the initially assigned position of each atom its full path is determined. We choose the velocity distribution to be a Gaussian distribution with standard deviation σ_{v} in 1D, which coincides with the distribution of a thermal gas, when we care about one dimension only and is therefore what one would expect from thermal atoms. Later, we will arrange the atoms in clusters of identical atoms. This will allow us to simulate the system for much higher atom numbers while still solving the same number of equations.

The atoms themselves are modeled as two-level systems and interact with the electric field of the cavity by emitting and absorbing photons with a rate $\frac{g^2}{\kappa}$, depicted on the left-hand side of figure 3.1. Furthermore, the atoms are subject to two incoherent processes: the spontaneous emission of photons with rate γ and the incoherent pump (discussed in section 2.4.1), where the atoms are pumped to an auxiliary level, but rapidly decay to the excited state $|e\rangle$, eventually allowing for population inversion. The coherent exchange of energy between atoms and the cavity field is the interaction described by the Tavis-Cummings hamiltonian discussed in section 2.2,

$$\hat{H} = \hbar\omega_{\mathrm{a}} \sum_m \sigma_m^{\mathrm{ee}} + \hbar\omega_{\mathrm{c}} \hat{a}^\dagger \hat{a} + \hbar g \sum_m f(x_m) \left(\sigma_m^{\mathrm{eg}} \hat{a} + \sigma_m^{\mathrm{ge}} \hat{a}^\dagger \right), \tag{3.1}$$
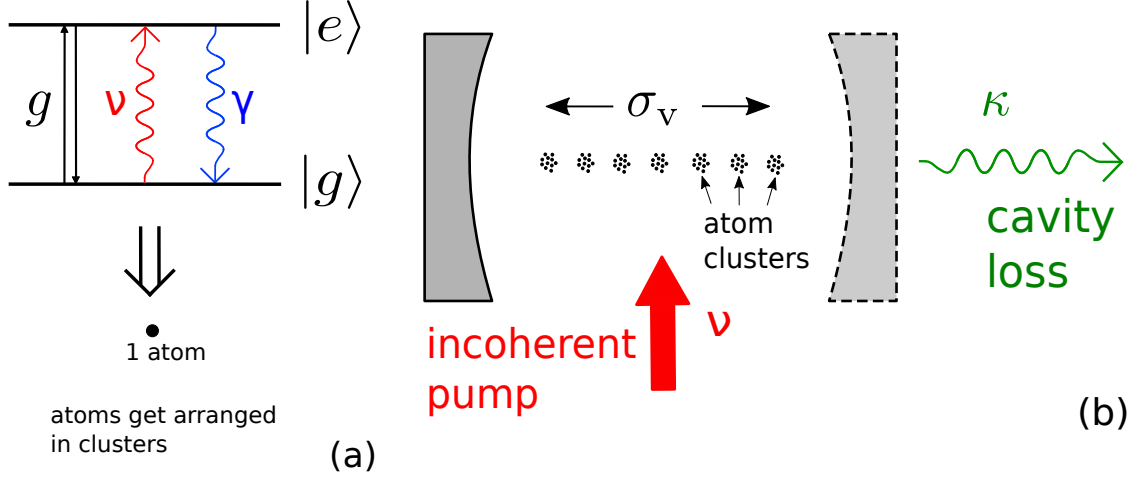
Figure 3.1.: *Overview of the processes and the simulated setup.* (a) Relevant processes for a single atom. (b) The atoms are grouped into clusters. The clusters move according to a gaussian velocity distribution with standard deviation σ_v. The atoms are incoherently pumped with a rate ν and photons leak out of the cavity with a rate κ.

where we have already included the position-dependent interaction strength due to the mode function $f(x_m)$. By transforming into a rotating frame according to section 2.3 we arrive at the Hamiltonian for our system, i.e.

$$H_{\text{int}} = \Delta a^\dagger a + g \sum_m f(x_m)(a^\dagger \sigma_m^{\text{ge}} + \sigma_m^{\text{eg}} a).$$

Choosing the initial expectation value $\langle \sigma_m^{\text{ee}} \rangle$ to be zero is equivalent to requiring all atoms to start in the ground state. Yet, we still need to include the dissipative processes. In our model we account for the spontaneous emission, the incoherent pump and the cavity losses. As discussed in section 2.4, for each incoherent process we have to identify the corresponding jump operator $\hat{c}$ and its rate of change in order to construct the term in Lindblad-form. The jump operator for the spontaneous emission is the atomic lowering operator σ^{ge} with the rate γ, while the incoherent pump is described by the atomic rising operator σ^{eg} with rate ν. Finally, we include the Lindblad term for the cavity loss by identifying the field annihilation operator $\hat{a}$ as the jump operator and κ as its rate. Written out in detail the Lindblad-terms read

$$\mathcal{L}_\gamma \rho = \frac{\gamma}{2} \sum_m (2\sigma_m^{\text{ge}} \rho \sigma_m^{\text{eg}} - \sigma_m^{\text{eg}} \sigma_m^{\text{ge}} \rho - \rho \sigma_m^{\text{eg}} \sigma_m^{\text{ge}}) \qquad \text{(spont. emission)}$$

$$\mathcal{L}_\nu \rho = \frac{\nu}{2} \sum_m (2\sigma_m^{\text{eg}} \rho \sigma_m^{\text{ge}} - \sigma_m^{\text{ge}} \sigma_m^{\text{eg}} \rho - \rho \sigma_m^{\text{ge}} \sigma_m^{\text{eg}}) \qquad \text{(spont. excitation)}$$

$$\mathcal{L}_\kappa \rho = \frac{\kappa}{2} (2a\rho a^\dagger - a^\dagger a \rho - \rho a^\dagger a) \qquad \text{(cavity loss)}.$$

Now, we are able to add these Lindblad-terms for the incoherent processes to the von Neumann equation describing the dynamics of the system under the Tavis-Cummings Hamiltonian, so that we arrive at the master equation for our system,

$$\dot{\rho} = -\frac{i}{\hbar}[H_{\text{int}}, \rho] + \mathcal{L}_{\gamma}\rho + \mathcal{L}_{\nu}\rho + \mathcal{L}_{\kappa}\rho \qquad (3.2)$$

Since we cannot solve the full master equation for more than a few atoms, we use the method of the cumulant expansion introduced in section 2.5 to obtain a set of differential equations that we can solve numerically in a realistic amount of computational time.

3.1. Mean Field

To keep things simple, let us first derive the equations of motion in mean field, meaning we approximate all operator product averages $\langle ab \rangle$ as products of operator averages $\langle a \rangle \langle b \rangle$. We are particularly interested in the photon number $\langle a^\dagger a \rangle$, but under our approximation we find $\langle a^\dagger a \rangle \approx \langle a^\dagger \rangle \langle a \rangle = \langle a \rangle^* \langle a \rangle = |\langle a \rangle|^2$. This suggests starting the derivation with the equation for $\langle a \rangle$, since we just need to take the absolute value squared of the time evolution of $\langle a \rangle$. Upon inserting the master equation for $\dot{\rho}$ we obtain

$$\dot{\langle a \rangle} = -\frac{i}{\hbar} \cdot \text{tr}\{a[H_{\text{int}}, \rho]\} + \underbrace{\text{tr}\{a \cdot \mathcal{L}_{\gamma}\rho\}}_{=0} + \underbrace{\text{tr}\{a \cdot \mathcal{L}_{\nu}\rho\}}_{=0} + \text{tr}\{a \cdot \mathcal{L}_{\kappa}\rho\}. \qquad (3.3)$$

We see immediately that $\text{tr}\{a \cdot \mathcal{L}_{\gamma}\rho\} = \text{tr}\{a \cdot \mathcal{L}_{\nu}\rho\} = 0$ because a commutes with all σ operators together with the invariance under cyclic permutation. Investigating the other terms yields (for $\Delta = 0$)

$$\text{tr}\{a[H_{\text{int}}, \rho]\} \propto \sum_m \text{tr}\{a[a^\dagger \sigma_m^{\text{ge}}, \rho]\}$$
$$= \sum_m \text{tr}\{aa^\dagger \sigma_m^{\text{ge}}\rho - a\rho a^\dagger \sigma_m^{\text{ge}}\}$$
$$= \sum_m \text{tr}\{[a, a^\dagger]\sigma_m^{\text{ge}}\rho\} = \sum_m \langle \sigma_m^{\text{ge}} \rangle$$

and

$$\text{tr}\{a \cdot \mathcal{L}_{\kappa}\rho\} = \frac{\kappa}{2} \cdot \text{tr}\{2aa\rho a^\dagger - aa^\dagger a\rho - a\rho a^\dagger a\}$$
$$= \frac{\kappa}{2} \cdot \text{tr}\{aa\rho a^\dagger - aa^\dagger a\rho\}$$
$$= \frac{\kappa}{2} \cdot \text{tr}\{\underbrace{[a^\dagger, a]}_{=-1} a\rho\} = -\frac{\kappa}{2} \cdot \langle a \rangle.$$

where we have used known commutators, once more the cyclic property of the trace and that a and all σ operators act on different Hilbert spaces. Altogether, we find the

following equation

$$\langle \dot{a} \rangle = -\left(\frac{\kappa}{2} + i\Delta\right)\langle a \rangle - ig \sum_m f(x_m)\langle \sigma_m^{\text{ge}} \rangle. \tag{3.4}$$

We notice that we have to derive the equation for $\langle \sigma_m^{\text{ge}} \rangle$ as well, in order to obtain a closed set. After additionally deriving the equation for $\langle \sigma_m^{\text{ee}} \rangle$ we are able to close the set by performing the above approximation $\langle ab \rangle \approx \langle a \rangle \langle b \rangle$. Realizing that for any operator $\hat{O}$ we have $\langle \hat{O}^\dagger \rangle = \langle \hat{O} \rangle^*$ we arrive at the set of differential equations for the mean field thatwesolve numerically,

$$\langle \dot{a} \rangle = -\left(\frac{\kappa}{2} + i\Delta\right)\langle a \rangle - ig \sum_m f(x_m)\langle \sigma_m^{\text{ge}} \rangle \tag{3.5a}$$

$$\langle \dot{\sigma}_m^{\text{ge}} \rangle = -\frac{\gamma + \nu}{2}\langle \sigma_m^{\text{ge}} \rangle + 2igf(x_m)\langle \sigma_m^{\text{ee}} \rangle\langle a \rangle \tag{3.5b}$$

$$\langle \dot{\sigma}_m^{\text{ee}} \rangle = -(\gamma + \nu)\langle \sigma_m^{\text{ee}} \rangle + igf(x_m)(\langle a \rangle^*\langle \sigma_m^{\text{ge}} \rangle - \langle \sigma_m^{\text{ge}} \rangle^*\langle a \rangle) + \nu. \tag{3.5c}$$

Until this point, we have treated each atom individually. As discussed above, we want to go to large atom numbers, and even in mean field we cannot numerically compute each of the atoms individually. Therefore, we group them into clusters of identical atoms: The index (m) is replaced by the index (m, i). The operator $\sigma_{m,i}$ acts on the i-th atom in the m-th cluster. The crucial simplification is to still treat the different clusters m individually, but require, that the atoms within a cluster are indistinguishable: $\langle \sigma_{m,i} \rangle = \langle \sigma_{m,j} \rangle$ for $i \neq j$. Now, let us have a look at how this changes our set of differential equations. The last two equations in 3.5 are copied once for each atom in the cluster (m). Therefore, we end up with K of these equations for a particular cluster, where K denotes the number of atoms in a cluster or the cluster size. But, as these atoms are indistinguishable, we just have the same equation K times. Obviously, we need to solve this equation only once. Altogether this means, that the last two equations stay the same and describe each atom (i) in its particular cluster (m) at the same time, as all atoms (i) are indistinguishable. For the first equation in 3.5, we now need to sum over all clusters (m), but also all atoms (i) within each cluster. But, as $\langle \sigma_{m,i} \rangle = \langle \sigma_{m,j} \rangle$, we conclude that the sum over i gives just a factor K: $\sum_{i=1}^{K} \langle \sigma_{m,i} \rangle = K \cdot \langle \sigma_m \rangle$. Therefore, the new equation reads

$$\langle \dot{a} \rangle = -\left(\frac{\kappa}{2} + i\Delta\right)\langle a \rangle - K \cdot ig \sum_{m=1}^{N_{\text{Cl}}} f(x_m)\langle \sigma_m^{\text{ge}} \rangle, \tag{3.6}$$

where the sum over m now goes up to the number of clusters N_{Cl}, instead of over all atoms individually as before. Altogether, the total atom number N is then the number of clusters N_{Cl} times the number of atoms per cluster K, $N = N_{\text{Cl}} \cdot K$. The source term $\sum_m f(x_m)\langle \sigma_m^{\text{ge}} \rangle$ becomes enhanced by the cluster size K, which demonstrates that the clusters now consist of K atoms, with each of these K atoms acting as a source. The

number of differential equations scales linearly with the number of individual clusters, in particular we obtain $1 + 2 \cdot N_{\text{Cl}}$ equations for N_{Cl} individual clusters in comparison to $2^{N_{\text{Cl}}} \cdot M_{\text{cutoff}}$ for the full quantum model (M_{cutoff} is the chosen photon cutoff). This linear scaling allows us to simulate many clusters, but we pay the price of having to neglect all quantum correlations.

3.2. Mixed Order Expansion

If we go to full second order, we have to derive equations for all operator products such as $\langle \sigma_j \sigma_n \rangle$ and we will eventually end up with quadratic scaling of the number of equations with the atom number. The idea behind using a mixed order expansion is to keep second order correlations between field and atoms of the type $\langle a\sigma \rangle$ only, but neglect the second order correlations between the atoms and approximate $\langle \sigma_j \sigma_n \rangle = \langle \sigma_j \rangle \langle \sigma_n \rangle$.

Once again, we are interested in the photon number $\langle a^\dagger a \rangle$. This time we derive the equation for the photon number directly, as we want to keep the second order correlations in the electromagnetic field. After similar, albeit longer, calculations than in the case for the mean field above, we find the equations for mixed order.

For some of the derivations, it is useful to know that $\text{Tr}\{\hat{O}[\hat{H}, \hat{\rho}]\} = 0$ if $[\hat{O}, \hat{H}] = 0$ because of the invariance of the trace under cyclic permutation: $\text{Tr}\{\hat{O}[\hat{H}, \hat{\rho}]\} = \text{Tr}\{\hat{O}\hat{H}\hat{\rho} - \hat{O}\hat{\rho}\hat{H}\} = \text{Tr}\{\hat{O}\hat{H}\hat{\rho} - \hat{H}\hat{O}\hat{\rho}\} = \text{Tr}\{[\hat{O}, \hat{H}]\rho\}$. The equations in mixed order

read

$$\langle \dot{a} \rangle = - \left(\frac{\kappa}{2} - i\Delta \right) \langle a \rangle - K \cdot ig \sum_m f(x_m) \langle \sigma_m^{\text{ge}} \rangle \tag{3.7a}$$

$$\langle \dot{a^\dagger a} \rangle = - \left(\kappa - 2i\Delta \right) \langle a^\dagger a \rangle + igK \sum_m f(x_m)(\langle a\sigma_m^{\text{eg}} \rangle - \langle a^\dagger \sigma_m^{\text{ge}} \rangle) \tag{3.7b}$$

$$\langle \dot{aa} \rangle = - \left(\kappa - 2i\Delta \right) \langle aa \rangle - 2igK \sum_m f(x_m) \langle a\sigma_m^{\text{ge}} \rangle \tag{3.7c}$$

$$\langle a\dot{\sigma}_m^{\text{eg}} \rangle = - \left(\frac{\gamma + \kappa + \nu}{2} - i\Delta \right) \langle a\sigma_m^{\text{eg}} \rangle + igf(x_m) \langle a^\dagger a \rangle - ig \sum_{j=1}^{N_{\text{Cl}}} \sum_{i=1}^{K} f(x_j) \langle \sigma_m^{\text{eg}} \sigma_{j,i}^{\text{ge}} \rangle$$
$$- 2igf(x_m) \langle a^\dagger a\sigma_m^{\text{ee}} \rangle \tag{3.7d}$$

$$\langle a\dot{\sigma}_m^{\text{ge}} \rangle = - \left(\frac{\gamma + \kappa + \nu}{2} - i\Delta \right) \langle a\sigma_m^{\text{ge}} \rangle - igf(x_m) \langle aa \rangle - ig \sum_{j=1}^{N_{\text{Cl}}} \sum_{i=1}^{K} f(x_j) \langle \sigma_m^{\text{ge}} \sigma_{j,i}^{\text{ge}} \rangle$$
$$+ 2igf(x_m) \langle aa\sigma_m^{\text{ee}} \rangle \tag{3.7e}$$

$$\langle \dot{\sigma}_m^{\text{ee}} \rangle = igf(x_m)(\langle a^\dagger \sigma_m^{\text{ge}} \rangle - \langle a\sigma_m^{\text{eg}} \rangle) - (\gamma + \nu) \langle \sigma_m^{\text{ee}} \rangle + \nu \tag{3.7f}$$

$$\langle \dot{\sigma}_m^{\text{ge}} \rangle = - \frac{\gamma + \nu}{2} \langle \sigma_m^{\text{ge}} \rangle - igf(x_m) \langle a \rangle + 2igf(x_m) \langle a\sigma_m^{\text{ee}} \rangle \tag{3.7g}$$

$$\langle a\dot{\sigma}_m^{\text{ee}} \rangle = - (\gamma + \nu) \langle a\sigma_m^{\text{ee}} \rangle - \frac{\kappa}{2} \langle a\sigma_m^{\text{ee}} \rangle + \nu \langle a \rangle - igf(x_m) \langle aa\sigma_m^{\text{eg}} \rangle$$
$$- ig \sum_{j=1}^{N_{\text{Cl}}} \sum_{i=1}^{K} f(x_m) \langle \sigma_m^{\text{ee}} \sigma_{j,i}^{\text{ge}} \rangle + igf(x_j) \langle a^\dagger a\sigma_m^{-} \rangle. \tag{3.7h}$$

Once again, we have already inserted the cluster size K where it belongs. For the first three equations in 3.7 we obtain an enhancement of the source term, similar to the first equation in mean field. The sixth and seventh equation are copied K times, similar to the last two equations in mean field. However, for the forth, fifth and last equation, we need to be a little more careful while evaluating the double sums, as we need to distinguish the cases $j \neq m$ and $j = m$: To evaluate the first double sum in the equation for $\langle a\sigma_m^{\text{eg}} \rangle$, we split the sum over (j) into two parts, namely $j \neq m$ and $j = m$. For the sum with $j \neq m$, we are in a similar situation as in the mean field above, we approximate $\langle \sigma_m^{\text{eg}} \sigma_{j,i}^{\text{ge}} \rangle$ as $\langle \sigma_m^{\text{eg}} \rangle \langle \sigma_{j,i}^{\text{ge}} \rangle$ and carry out the sum over i which gives us a factor of K,

$$\sum_{j \neq m} \sum_{i=1}^{K} f(x_j) \langle \sigma_m^{\text{eg}} \sigma_{j,i}^{\text{ge}} \rangle = \sum_{j \neq m} \sum_{i=1}^{K} f(x_j) \langle \sigma_m^{\text{eg}} \rangle \langle \sigma_{j,i}^{\text{ge}} \rangle = K \cdot \langle \sigma_m^{\text{eg}} \rangle \sum_{j \neq m} f(x_j) \langle \sigma_j^{\text{ge}} \rangle. \tag{3.8}$$

The sum with $j = m$ describes the correlations within a cluster,

$$\sum_{j=m}\sum_{i=1}^{K} f(x_j)\langle\sigma_m^{\mathrm{eg}}\sigma_{j,i}^{\mathrm{ge}}\rangle = \sum_{i=1}^{K} f(x_m)\langle\sigma_m^{\mathrm{eg}}\sigma_{m,i}^{\mathrm{ge}}\rangle. \tag{3.9}$$

In order to simplify further we have a closer look at the expression $\langle\sigma_m^{\mathrm{eg}}\sigma_{m,i}^{\mathrm{ge}}\rangle$. Here, σ_m^{eg} is the operator acting on a particular atom in cluster (m). One particular (i) in this sum will be the very same atom as the atom, on which σ_m^{eg} acts and then we simplify $\langle\sigma_m^{\mathrm{eg}}\sigma_{m,i}^{\mathrm{ge}}\rangle = \langle\sigma_m^{\mathrm{ee}}\rangle$. For all other (i) different from that particular i, the operators do not act on the same atom and we therefore approximate $\langle\sigma_m^{\mathrm{eg}}\sigma_{m,i}^{\mathrm{ge}}\rangle = \langle\sigma_m^{\mathrm{eg}}\rangle\langle\sigma_m^{\mathrm{ge}}\rangle$. This term appears $K-1$ times, as there are $K-1$ atoms in a cluster different from a particular atom. Altogether we have for the sum $j = m$

$$\sum_{i=1}^{K} f(x_m)\langle\sigma_m^{\mathrm{eg}}\sigma_{m,i}^{\mathrm{ge}}\rangle = (K-1)\cdot f(x_m)\langle\sigma_m^{\mathrm{eg}}\rangle\langle\sigma_m^{\mathrm{ge}}\rangle + f(x_m)\langle\sigma_m^{\mathrm{ee}}\rangle. \tag{3.10}$$

For the second and third double sum in 3.7 we proceed similarly. However, the last term where both operators act on the very same atom vanishes, as $\sigma_m^{\mathrm{ge}}\sigma_m^{\mathrm{ge}} = 0$ and $\sigma_m^{\mathrm{ee}}\sigma_m^{\mathrm{ge}} = 0$. Putting it all together, the double sums in 3.7 can be evaluated as

$$\sum_{ji} f(x_j)\langle\sigma_m^{\mathrm{eg}}\sigma_{j,i}^{\mathrm{ge}}\rangle = K\cdot\langle\sigma_m^{\mathrm{eg}}\rangle\sum_{j\neq m} f(x_j)\langle\sigma_j^{\mathrm{ge}}\rangle + (K-1)\cdot f(x_m)\langle\sigma_m^{\mathrm{eg}}\rangle\langle\sigma_m^{\mathrm{ge}}\rangle + f(x_m)\langle\sigma_m^{\mathrm{ee}}\rangle$$

$$\sum_{ji} f(x_j)\langle\sigma_m^{\mathrm{ge}}\sigma_{j,i}^{\mathrm{ge}}\rangle = K\cdot\langle\sigma_m^{\mathrm{ge}}\rangle\sum_{j\neq m} f(x_j)\langle\sigma_j^{\mathrm{ge}}\rangle + (K-1)\cdot f(x_m)\langle\sigma_m^{\mathrm{ge}}\rangle\langle\sigma_m^{\mathrm{ge}}\rangle + 0$$

$$\sum_{ji} f(x_j)\langle\sigma_m^{\mathrm{ee}}\sigma_{j,i}^{\mathrm{ge}}\rangle = K\cdot\langle\sigma_m^{\mathrm{ee}}\rangle\sum_{j\neq m} f(x_j)\langle\sigma_j^{\mathrm{ge}}\rangle + (K-1)\cdot f(x_m)\langle\sigma_m^{\mathrm{ee}}\rangle\langle\sigma_m^{\mathrm{ge}}\rangle + 0.$$

All averages over products of three operators can be rewritten in terms of averages over products of at most two operators, as introduced in section 2.5, such that

$$\langle abc\rangle \approx \langle ab\rangle\langle c\rangle + \langle ac\rangle\langle b\rangle + \langle cb\rangle\langle a\rangle - 2\langle a\rangle\langle b\rangle\langle c\rangle. \tag{3.11}$$

For the sake of better readability we shall refrain from carrying out all the expansions in the above set of differential equations. In the end, we are able to close the set with having $3 + 5\cdot N_{\mathrm{Cl}}$ equations for N_{Cl} individual clusters. So, the number of equation still scales linearly as in the case of the mean field. This time however, quantum correlations between atoms and photons are included.

There is an additional idea to simplify the equations: we never specify the phase for the system, if we start with all expectation values being zero. The incoherent processes have a random phase, and as the master equation sums over all possibilities the average is zero. This means, that only the phase invariant terms survive. From the set of equations above only three are phase invariant and we end up with $1 + 2\cdot N_{\mathrm{Cl}}$ equations

for N_{Cl} clusters,

$$\langle a^\dagger \dot{a}\rangle = -\left(\kappa - 2i\Delta\right)\langle a^\dagger a\rangle + igK\sum_m f(x_m)(\langle a\sigma_m^{\mathrm{eg}}\rangle - \langle a^\dagger \sigma_m^{\mathrm{ge}}\rangle) \tag{3.12a}$$

$$\langle a\dot{\sigma}_m^{\mathrm{eg}}\rangle = -\left(\frac{\gamma + \kappa + \nu}{2} - i\Delta\right)\langle a\sigma_m^{\mathrm{eg}}\rangle + igf(x_m)\langle a^\dagger a\rangle - igK\cdot\langle\sigma_m^{\mathrm{eg}}\rangle\sum_{j\neq m} f(x_j)\langle\sigma_j^{\mathrm{ge}}\rangle$$
$$- ig(K-1)\cdot f(x_m)\langle\sigma_m^{\mathrm{eg}}\rangle\langle\sigma_m^{\mathrm{ge}}\rangle - igf(x_m)\langle\sigma_m^{\mathrm{ee}}\rangle - 2igf(x_m)\langle a^\dagger a\sigma_m^{\mathrm{ee}}\rangle \tag{3.12b}$$

$$\langle\dot{\sigma}_m^{\mathrm{ee}}\rangle = igf(x_m)(\langle a^\dagger\sigma_m^{\mathrm{ge}}\rangle - \langle a\sigma_m^{\mathrm{eg}}\rangle) - (\gamma + \nu)\langle\sigma_m^{\mathrm{ee}}\rangle + \nu. \tag{3.12c}$$

Considering the phase invariant terms only we arrive at the same computational complexity as in the case of mean field.

Chapter 4.

Simulation of the laser dynamics

In chapter 2 we have discussed the underlying formulas and concepts governing the dynamics of a single mode multi-atom laser and in chapter 3 we have particularized the relevant formulas to our specific model and derived a set of differential equations approximating the dynamics. Now, we solve these equations numerically for different parameters and have a discuss the results.

4.1. Simulated photon number trajectories
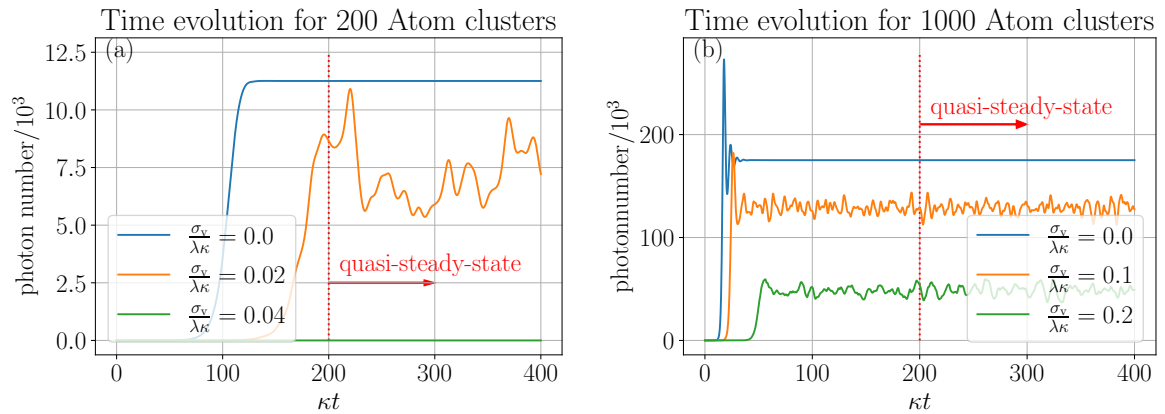
Figure 4.1.: *Example of the photon number time evolutions for different velocity spreads σ_v in a mean field approximation.* (a) Photon number evolution for different σ_v for 200 atom clusters. (b) Mean photon number evolution for different σ_v for 1000 atom clusters. After a certain time, the system reaches its quasi steady state and the photon number fluctuates around its value. The fluctuations, however, become smaller if we divide the velocity distribution into a larger number of atom clusters. The other parameters are: $K = 1000$, $\nu = 0.5$, $\gamma = 10^{-8}$, $\Delta = 0$, $g = 1.36 \cdot 10^{-3}$, $\kappa = 1$.

Let us first investigate some example trajectories in order to get a general idea of how the system behaves. Figure 4.1 shows a few photon number evolutions in mean field for

velocity distributions with different standard deviations σ_v. On the left-hand side we show the system using a division in 200 atom clusters, while on the right-hand side we go as high as 1000 atom clusters. We start with small initial values different from zero to introduce an initial phase, so either we choose $\langle a \rangle(t = 0) \neq 0$ or $\langle \sigma_m^\mathrm{ge} \rangle(t = 0) \neq 0$. We always end up with very similar trajectories, no matter which of the initial values we choose to be nonzero or by how much. From the graphs we see, that lower values for σ_v, i.e. lower temperatures allow the system to reach its quasi steady state faster and higher values lead to the system reacting more slowly. For atoms at rest, i.e. $\sigma_\mathrm{v} = 0$, we end up with a constant steady state photon number. (blue trajectories). In contrast, moving atoms will always result in photon number fluctuations around a certain value. Moreover, the lower the standard deviation σ_v of the velocity distribution, the higher the photon number in the cavity.

In the following sections we will have a closer look at this phenomenon, which can be explained by the Doppler effect: faster atoms see the photons shifted up or down in frequency, depending on if they are moving towards or away from them. This frequency difference will suppress their interaction with the cavity field. If we choose σ_v too large there will be virtually no photons in the cavity (green trajectory in the left graph). Lastly, we see that choosing a larger number of atom clusters leads to the quasi steady state faster and, crucially, also to less fluctuations around its value (compare the orange trajectories in the right and left graph). However, we have to pay for this clearer picture with more atom clusters, therefore a larger number of equations and as a result, we need more time to compute the dynamics numerically. Ideally, we would simulate each atom individually, but this is, as already discussed, not feasible.

In order to simulate a homogeneous density we equidistantly place the atoms along the cavity mode and distribute them equally over one wavelength. When the atoms move with a certain velocity, they will, sooner or later (depending on their initial position), sample an average of the mode function. The effective interaction strength $\sum_m g_m^2$ (with $g_m = g \cdot f(x_m)$) is then equal to $\frac{1}{2} \cdot \sum_m g^2$, as $f = \cos$ and the average of $\cos^2$ over a period is $\frac{1}{2}$. In figure 4.2 we depict the situation of all atoms starting at the maximum of the mode function. The blue trajectory depicts the situation for fixed atoms, where we end up with roughly 200 photons. As soon as we increase σ_v just a little (orange trajectory), the initial photon number follows the blue trajectory, but, as the atoms start to distribute themselves equally over a period of the mode function, begins to drop down to about 100 photons. If we increase σ_v further we start to see less and less photons appear in the cavity, which is due to the Doppler effect. To isolate the influence of the Doppler effect on the photon number from the influence of the initial positions of the atom, we need to make sure that the effective interaction strength for fixed atoms and for moving atoms stays the same. For this reason we place the atoms equidistantly and equally distributed over one period of the mode function.

Now let us study the influence of different numbers of atom clusters in order to find a suitable value for our simulations. To this end, we simulate a total number of
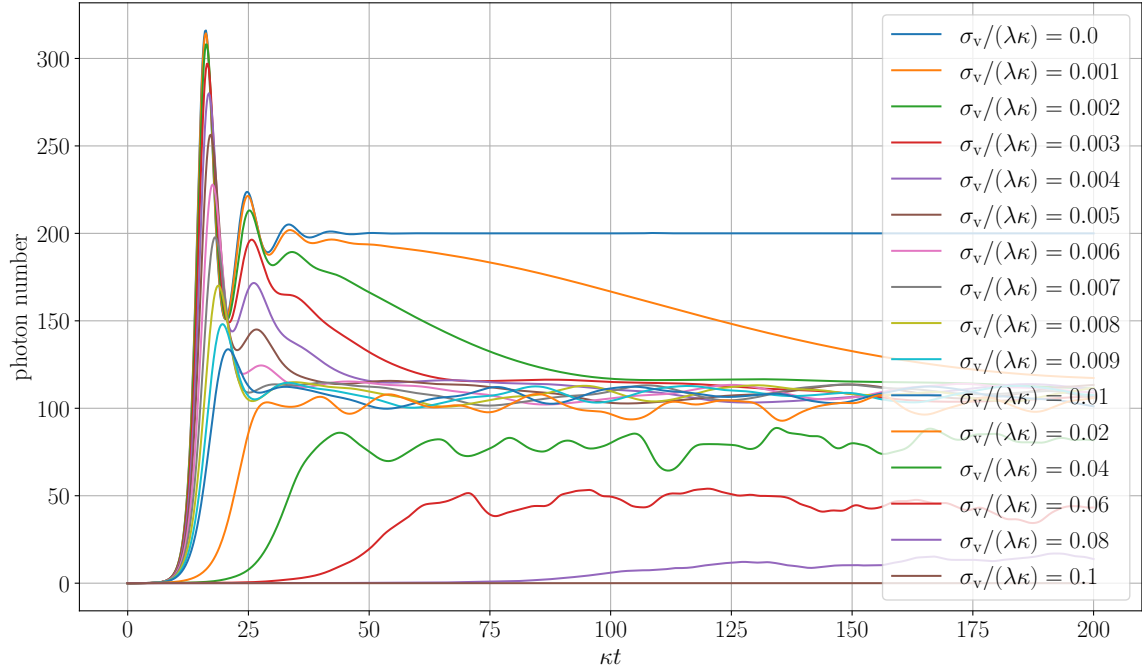
Figure 4.2.: *Photon number evolution with all atoms initially at a mode function maximum (antinode).* Only for $\sigma_v = 0$ (optimal coupling, blue trajectory) the photon number stays at around 200. As soon as we allow for motion, the photon number will eventually drop to about half of the value. The trajectories that do not even reach this level are those with such large a value of σ_v that the Doppler effect suppresses the interaction between atoms and photons. The other parameters are $K = 1$, $\nu = 0.5$, $\gamma = 10^{-8}$, $\Delta = 0$, $g = 0.05$, $\kappa = 1$.

10^6 atoms, grouped into 1000 clusters (1000 atoms per cluster), in 400 clusters (2500 atoms per cluster), in 200 clusters (5000 atoms per cluster) and in 50 clusters (20000 atoms per cluster) and depict the results in figure 4.3. This way, all differences in the results can be traced back to the different groupings of the atoms. On the left-hand side of figure 4.3 we compare the results for two particular values of σ_v, while on the right-hand side we average over many trajectories (see details in section 4.2) to arrive at an average photon number in quasi steady state depending on σ_v. As we can see from the left part of the figure, for small σ_v the different trajectories fluctuate around the same value, whereas for larger σ_v upon close inspection one sees that the value of the brown trajectory (for the lowest number of atom clusters: 50 corresponding to 2000 atoms per cluster) fluctuates much more. When averaging over many trajectories these fluctuations average out for the most part and we see that the results agree for different cluster numbers. However, for a number of clusters as low as 50, we observe noticeable deviations, especially for large values of σ_v. For small σ_v the three graphs are virtually indistinguishable. One has to keep in mind that, in principle, we would have to treat each atom individually, which would require simulating 10^6 atom clusters with cluster

size 1. But, given these results, we can estimate that the difference is not too big. The above considerations lead us to using an atom cluster number of 400 for the following simulations. For higher order expansions we might want to reduce the number further while keeping in mind to average over more trajectories so that we arrive at a smooth graph.
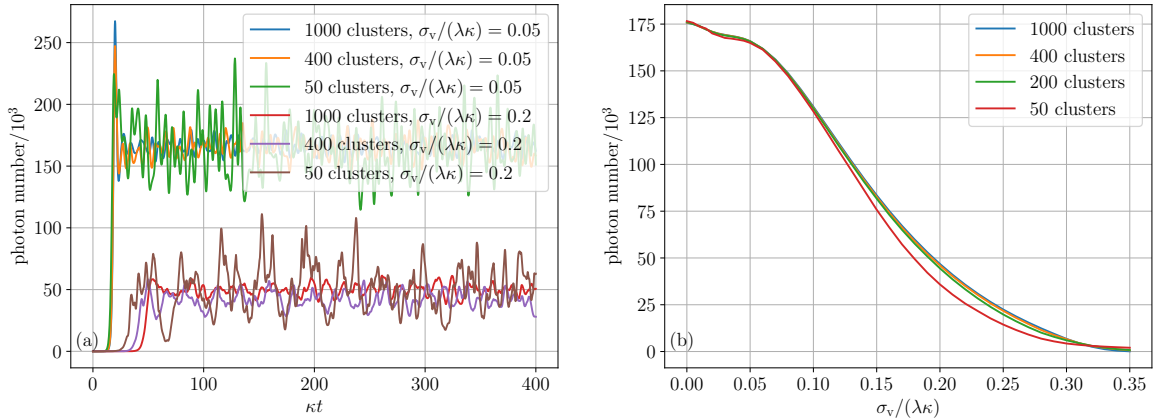
Figure 4.3.: *Comparison of simulations using different numbers of atom clusters with the same total number of atoms* 10^6. (a) Some example trajectories. (b) Photon number in quasi-steady-state averaged over many trajectories. We always use the same parameters, in particular the same total number of atoms. We observe only small differences, especially for large σ_{v}. The other parameters are $\nu = 0.5$, $\gamma = 10^{-8}$, $\Delta = 0$, $g = 1.36 \cdot 10^{-3}$, $\kappa = 1$.

4.2. Photon number dependence on temperature

As mentioned in the previous section, now, we look more closely at how the photon number in quasi steady state behaves as a function of σ_{v}. As the atoms move through maxima and nodes of the mode function, the photon number fluctuates. In order to get a meaningful result, we average over time letting the system evolve longer and average over all the values of the trajectories after the system reaches its quasi steady state. For typical trajectories in the parameter range we are interested in we conclude that $\kappa t = 200$ is a good time at which the system has reached its quasi steady state (all rates are measured in κ, therefore all times are measured in $\frac{1}{\kappa}$, more details on this in appendix A). However, we could still by chance choose a particular velocity distribution, that incidentally has more or less photons compared to a typical velocity distribution with the same standard deviation σ_{v}. To minimize this effect we initialize our system with 50 different random Gaussian distributions (with the same standard deviation), let them evolve and calculate an average once more. For a better comparison we always use the same 50 random Gaussian distributions. In summary, to get a quasi steady state value for a certain σ_{v} we average over a lot of trajectories with different random

velocity distributions and over the fluctuations of each trajectory.

This way, we are able to average out effects stemming from the fluctuations in each trajectory and effects from certain special distributions. These quasi steady state values for the photon number are calculated for a list of σ_v-values, eventually leading to a graph such as 4.4. To compare the results for different σ_v we use the same probability distribution for each value (more on this in appendix B). Moreover, when we want to simulate the system for different atom numbers, we alter the cluster size instead of the number of clusters for better comparability.
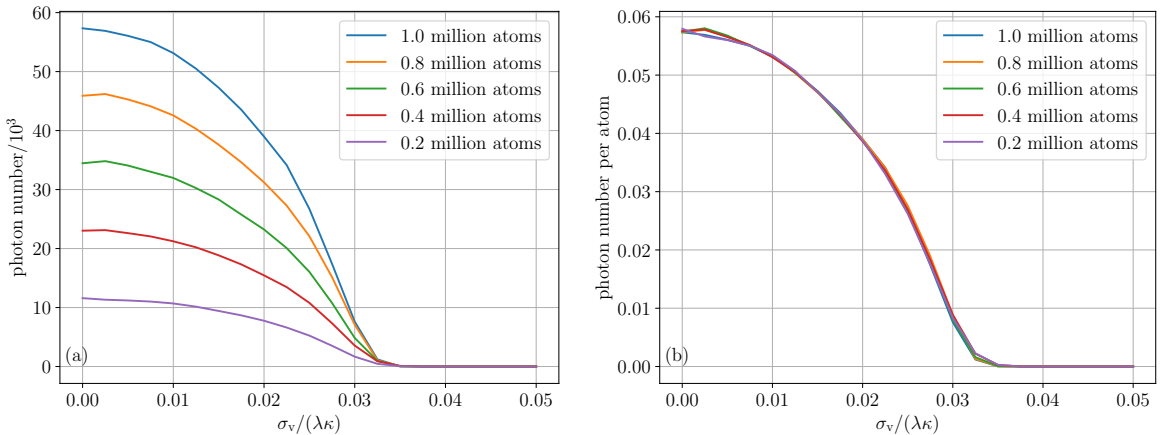
Figure 4.4.: *Quasi steady state photon numbers (mean field) as a function of the standard deviation of the velocity distribution σ_v with fixed collective cooperativity parameter.* (a) Absolute photon numbers. For more atoms, we also end up with more photons. (b) Photon number per atom. The curves for the photon number almost perfectly align. The maximum photon number always appears at $\sigma_v = 0$ or very small σ_v. With increasing σ_v the photon number drops due to the Doppler effect, to a point where there are no longer any photons inside the cavity. The other parameters are $\nu = 0.5$, $\gamma = 10^{-8}$, $\Delta = 0$, $g^2 \cdot N = 0.375$, $\kappa = 1$.

In figure 4.4, the result of the above procedure is depicted. We use the same parameters, except for the atom number N and the interaction strength g. However, we vary g in such a way, that the collective cooperativity parameter $\frac{g^2 N}{\kappa \gamma}$ is constant. On the left-hand side we depict the absolute number of photons for different atom numbers (by choosing different cluster sizes), while on the right-hand side the y-axis shows the photon numbers per atom. As we can see on the left, for more atoms we end up with more photons in general, even though the interaction strength becomes smaller (as $g^2 N = \text{const.}$). The interesting results are displayed on the right-hand side, where, if we choose the photon number per atom instead of the absolute photon numbers, the curves almost perfectly align.

It seems that the number of photons per atom is linearly correlated with the parameter $g^2 N$, which also means that the total number of photons scales with $g^2 N^2$. Looking at

the right hand side, we also notice some properties of the curves: the maximum number of photons is always achieved for very small velocities, usually for $\sigma_v = 0$. For larger velocities the photon numbers begin to drop until a point, where we no longer have photons in the cavity if we choose σ_v too large. This behaviour can be explained by the Doppler effect: the moving atoms see the photons with a different frequency and are therefore detuned from the photon frequency, making the interaction between them harder. The faster the atoms are, the higher the detuning is, until a point where the photons no longer interact with the atoms.
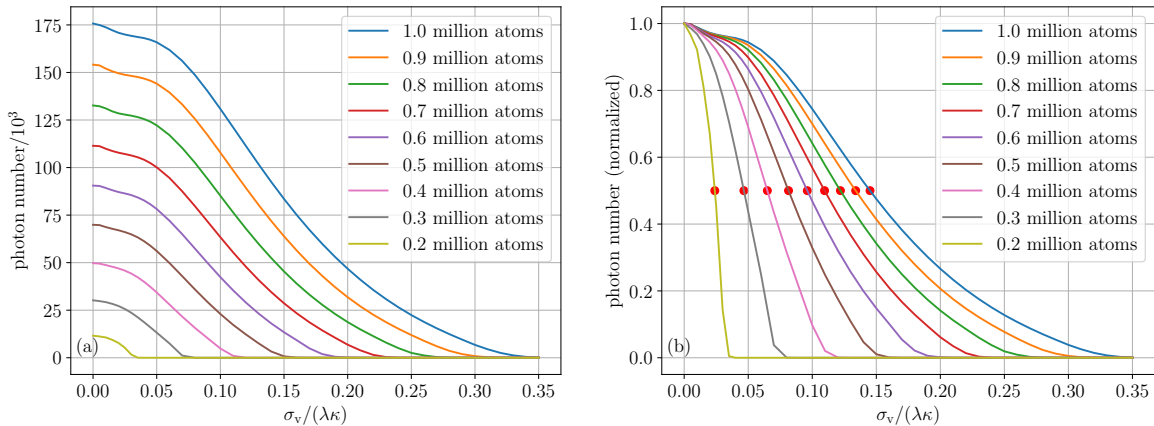
Figure 4.5.: *Quasi steady state photon numbers (mean field) as a function of the standard deviation of the velocity distribution σ_v with fixed g, but variable atom numbers.* (a) Absolute photon number. (b) Photon number normalized to $\sigma_v = 0$ (maximum). The red dots indicate the value at which the curves have dropped to half of their initial value. Now, the curves on the right hand side do not longer align when normalized. Larger atom numbers allow for larger possible values of σ_v, while maintaining a lot of photons inside the cavity. The parameters are $N_{Cl} = 400$, $\nu = 0.5$, $\gamma = 10^{-8}$, $\Delta = 0$, $g = 0.00136$, $\kappa = 1$.

Now that we have investigated the situation of keeping the collective cooperativity parameter constant, let us look at the influence the atom number exerts on the system, while fixing the other system parameters. As mentioned above, for changing the atom number we alter the cluster size instead of the number of clusters for better comparability. Once again, we average over a lot of trajectories to get rid of the effects a single initial velocity distributions and we average over each trajectory to get rid of the fluctuations. The results of this calculations are depicted in figure 4.5. On the right hand side of figure 4.5 one can see the photon numbers, this time normalized to the maximum photon number at $\sigma_v = 0$ for different cluster sizes. Qualitatively, they all look very similar to the graphs before. Crucially however, they do not longer align with each other. When using more atoms the curves decrease later, at larger σ_v and the threshold value, at which no photons are in the cavity anymore, increases for larger atom numbers. In order to compare how soon the curves drop, for each curve we determine the threshold

value of σ_v at which the number of photons has decreased to half of the maximum at $\sigma_\mathrm{v} = 0$ (indicated by the red dot) and depict it in figure 4.6. One can clearly see that for larger photon numbers the threshold value of σ_v increases. The dependency is almost linear, upon closer inspection it looks like a polynomial behaviour with an exponent slightly below 1. These results suggest that instead of trying to minimize the velocity distribution (and thereby the temperature), which can be experimentally challenging, one could increase the number of atoms in order to still realize decently large photon numbers. However, it remains to be seen which effects this has on the linewidth of the resulting output light.

So far we have simulated the system in mean field (lowest order) only as this is numerically the fastest. However, as discussed in section 3.2, in the so-called mixed order we can include all second order correlations with the exception of atom-atom correlations, and still end up with a set of differential equations that scales linearly with the system size, i.e. the number of atom clusters. The results that we obtain from these calculations are shown in figure 4.7. For comparison, we additionally depict the mean field results as a reference. The dotted lines represent the data calculated in mixed order. On the left hand side of the figure we can see that the results in mean field and mixed order agree very well and the same results as in mean field are to be expected. To see the difference between these two orders of

Figure 4.6.: *Dependence of the threshold value of the velocity spread σ_v on the number of atoms. Larger atom numbers allow for larger velocity spreads (i.e. temperature) while still having photons inside the cavity. The parameters are the same as for the results in figure 4.5.*

approximation one has to zoom in to the graph to make the separation of the lines visible as shown on the right-hand-side of figure 4.7.
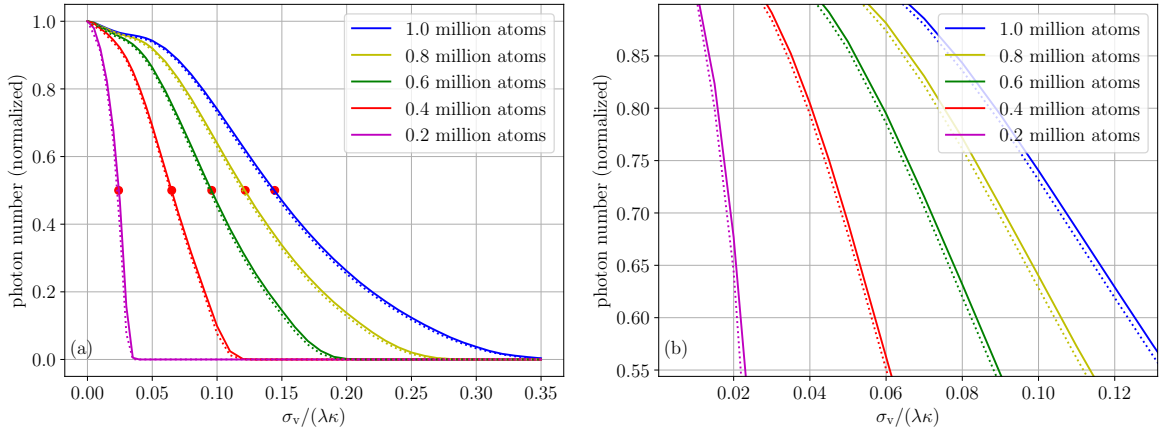
Figure 4.7.: *Quasi steady state photon numbers as a function of the standard deviation of the velocity distribution σ_{v} with fixed g, but variable atom numbers.* (a) Normalized photon numbers in mean field (solid line) and mixed order (dotted line). (b) Zoomed in region of the plot on the left. The solid line represents the results in mean field from above, the dotted line shows the data calculated from mixed order. The differences are minute, visually distinguishable only upon zooming in. The parameters are $N_{\mathrm{Cl}} = 400$, $\nu = 0.5$, $\gamma = 10^{-8}$, $\Delta = 0$, $g = 0.00136$, $\kappa = 1$.

Now, the question arises how the results would change upon using second order, where we keep the quantum correlations between the atoms. Yet, to be able to simulate the system we have to significantly reduce the number of clusters N_{Cl}. A comparison of the absolute photon numbers in mean field (solid line, $N_{\mathrm{Cl}} = 400$), mixed order (dotted line, $N_{\mathrm{Cl}} = 400$) and second order (dashed line, $N_{\mathrm{Cl}} = 25$) is depicted on the left-hand side of figure 4.8. We see, that for low σ_{v} the results agree, but for higher σ_{v} the result in second order drops below the results for the other orders. This is, however, due to the choice of using different numbers of atom clusters (compare with figure 4.3, where a lower number of clusters also leds to slightly different results): on the right-hand side we use $N_{\mathrm{Cl}} = 25$ clusters and the results in different expansion orders agree. From these two graphs we conclude, that mean field and mixed order yield similar results as second order, but we aim at simulating a large number of atom clusters, which we can only do in mean-field and mixed order.
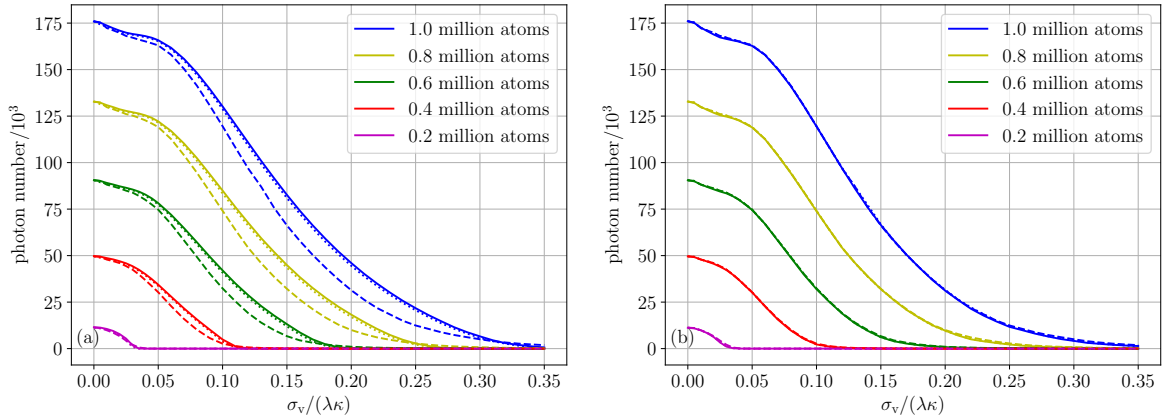
Figure 4.8.: *Absolute photon numbers using different orders in the cumulant expansion.* The solid line represents mean field, the dotted line is mixed order and the dashed line depicts the result in second order. (a) We use $N_{\text{Cl}} = 400$ clusters for mean field and mixed order, but only $N_{\text{Cl}} = 25$ clusters for second order. (b) We use $N_{\text{Cl}} = 25$ clusters for mean field, mixed order and second order. On the left, for small σ_{v} the results agree very well, but for larger σ_{v} the results in second order differ slightly from the other results. These differences come from using fewer clusters for second order (compare with results in 4.3): on the right, where we use the same cluster sizes for all expansions, all orders agree with each other. The other parameters are $\nu = 0.5$, $\gamma = 10^{-8}$, $\Delta = 0$, $g = 0.00136$, $\kappa = 1$.

4.3. Comparison of different cumulant expansion orders

So far, when simulating the system in mixed order, we have always used all $3 + 5 \cdot N_{\text{Cl}}$ equations as discussed in section 3.2. To compare with the mean field, we have used inhomogeneous initial conditions, similar to what we have done in mean field. These results, mean field and full mixed order with inhomogeneous initial conditions, agree very nicely as seen in the previous section. Now, the question arises, if we could use the reduced mixed order with $1 + 2 \cdot N_{\text{Cl}}$ equations to save some computational time. A simple simulation for $\sigma_{\text{v}} = 0$ reveals that the result differs noticeably compared to the result for full mixed order with inhomogeneous initial conditions and therefore it also differs from the mean field. To investigate this curious result, again, we look at the average photon number in quasi steady state for different atom numbers and different velocities. The result is depicted in figure 4.9. The solid line depicts the result in mean field/full mixed order with inhomogeneous initial conditions, while the dotted line shows the result for reduced mixed order. As we can see, they do not only differ for $\sigma_{\text{v}} = 0$, but in fact for all possible σ_{v} and all depicted atom numbers, and also by quite large a margin.

One could argue that there might have been a mistake in the program for the reduced mixed order. To check this we use the program for full mixed order, but with homogenous initial conditions, i.e. we set all initial values to zero, which should be mathematically
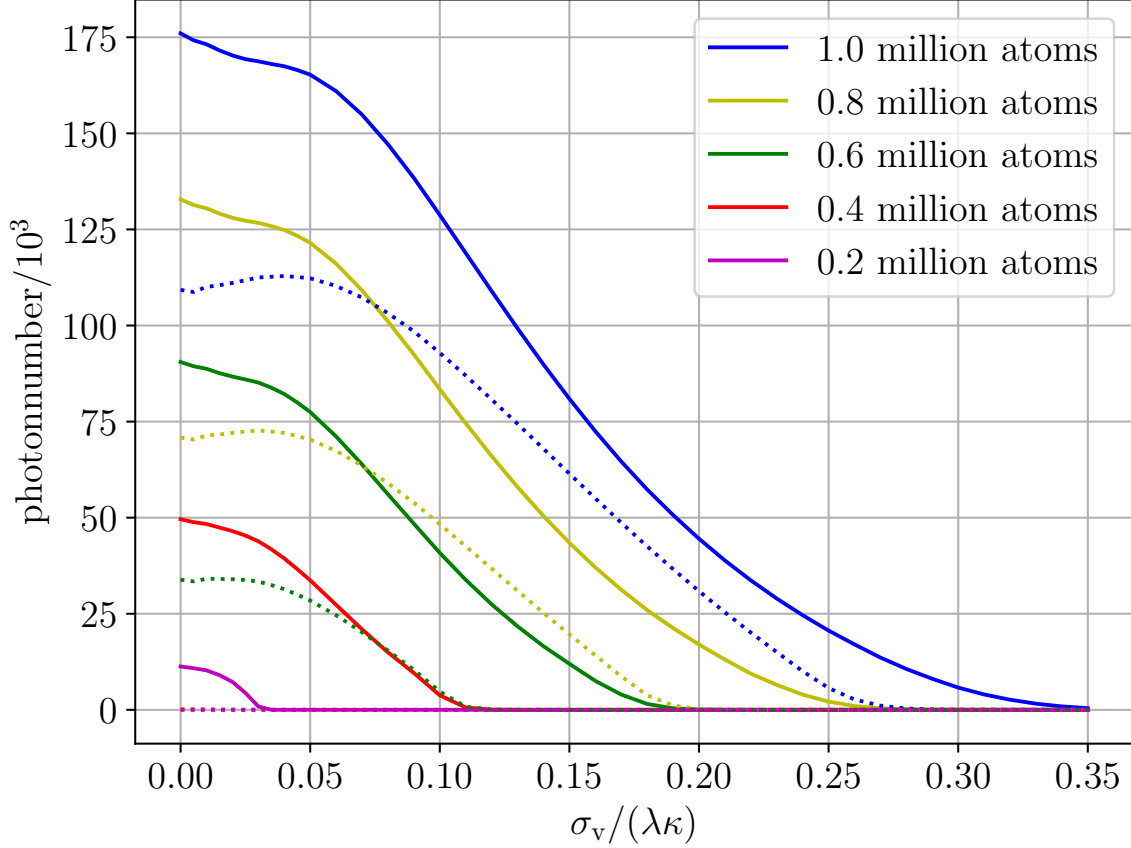
Figure 4.9.: *Difference between full and reduced mixed order.* The colour indicates the number of atoms. A solid line depicts the result in mean field/full mixed order with inhomogeneous initial condition, while the dotted line shows the result for reduced mixed order. The results disagree substantially at small σ_v. The parameters are $N_\mathrm{Cl} = 400$, $\nu = 0.5$, $\gamma = 10^{-8}$, $\Delta = 0$, $g = 0.00136$, $\kappa = 1$.

equivalent to the reduced mixed order: Looking at the equations for reduced mixed order

$$\langle a^\dagger a \rangle = -\left(\kappa - 2i\Delta\right)\langle a^\dagger a \rangle + igK \sum_m f(x_m)(\langle a\sigma_m^\mathrm{eg}\rangle - \langle a^\dagger \sigma_m^\mathrm{ge}\rangle)$$

$$\langle \dot{a\sigma_m^\mathrm{eg}} \rangle = -\left(\frac{\gamma + \kappa + \nu}{2} - i\Delta\right)\langle a\sigma_m^\mathrm{eg}\rangle + igf(x_m)\langle a^\dagger a \rangle - igK \cdot \langle\sigma_m^\mathrm{eg}\rangle \sum_{j\neq m} f(x_j)\langle\sigma_j^\mathrm{ge}\rangle$$

$$- ig(K-1) \cdot f(x_m)\langle\sigma_m^\mathrm{eg}\rangle\langle\sigma_m^\mathrm{ge}\rangle - igf(x_m)\langle\sigma_m^\mathrm{ee}\rangle - 2igf(x_m)\langle a^\dagger a\sigma_m^\mathrm{ee}\rangle$$

$$\langle \dot{\sigma_m^\mathrm{ee}} \rangle = igf(x_m)(\langle a^\dagger\sigma_m^\mathrm{ge}\rangle - \langle a\sigma_m^\mathrm{eg}\rangle) - (\gamma + \nu)\langle\sigma_m^\mathrm{ee}\rangle + \nu,$$

we see that these equations form a closed set, except for the terms $\langle\sigma_m^\mathrm{eg}\sigma_j^\mathrm{ge}\rangle$ and $\langle a^\dagger a\sigma_m^\mathrm{ee}\rangle$ in the second equation. We get rid of them if we set all single expectation values (except

for $\langle \sigma_m^{\text{ee}} \rangle$) to zero: we approximate $\langle \sigma_m^{\text{eg}} \sigma_j^{\text{ge}} \rangle$ as $\langle \sigma_m^{\text{eg}} \rangle \langle \sigma_j^{\text{ge}} \rangle$ for $j \neq m$ (for $j = m$ we end up with $\langle \sigma_m^{\text{ee}} \rangle$) and we now have only single operator expectation values, which are initialized as zero by choosing homogeneous initial conditions. Similarly, we approximate $\langle a^\dagger a \sigma_m^{\text{ee}} \rangle$ using the cumulant expansion formula introduced in section 2.5 as products of at most two-operator expectation values. The first term can now be rewritten in terms of $\langle a^\dagger a \rangle$ and $\langle \sigma_m^{\text{ee}} \rangle$, while the other terms are products with at least one term like $\langle a \rangle$ or $\langle a^\dagger \rangle$, which are initialized as zero by choosing homogeneous initial conditions. Looking at the full equations we also see that in the equations for the expectation values of the phase dependent terms all source terms are again phase dependent, meaning that if we initially set all phase dependent terms to zero, they will never be become nonzero.

The results from the full mixed order with homogeneous initial conditions and from the reduced mixed order agree completely, verifying the above mathematical considerations and suggesting that there has been no error in the program code. It seems that choosing the initial condition to be either inhomogeneous or homogeneous makes all the difference. This seems very curious, as the effect of the initial conditions usually fades out and one eventually ends up in a similar state for systems with a quasi steady state. To further investigate the influence of the initial conditions on the system we look at all expectation values of the system, not just the photon number. Surprisingly, for very small atom numbers it turns out that the initial conditions fade out and we have the same result for reduced mixed order and full mixed order with inhomogeneous initial conditions in contrast to the result for large atom numbers depicted in figure 4.9. Larger atom numbers eventually cause the initial conditions not to fade out anymore. The threshold, at which this damping vanishes, is investigated in figures 4.10 and 4.11. Figure 4.10 shows the system before we reach the threshold, while figure 4.11 depicts the results after crossing the threshold. We look at each expectation value, but for all operators indexed with m we only depict one cluster ($m = 1$), as the results are very similar for other clusters. The initial condition reads $0.1 + 0.0 \cdot i$. We choose such a high (real) value to show that it still damps out. The blue line depicts the real value, while the orange line represents the imaginary part. In figure 4.10 one can easily see that all the values eventually damp out to 0, regardless of the initial condition, with the exception being, as expected, the phase-invariant terms $\langle a^\dagger a \rangle$, $\langle a \sigma^{\text{eg}} \rangle$ and $\langle \sigma^{\text{ee}} \rangle$. For this result we have used 40 clusters and a cluster size of 250. However, just increasing the cluster size to 260 in figure 4.11, we see something completely different: suddenly, the initial conditions do not damp out anymore. We have crossed a threshold. The phase dependent terms now contribute to the time evolution and change the results. One might wonder, what happens in between the cluster sizes 250 and 260. The answer is that already at 251 the initial condition does not damp out anymore, but one has to simulate the system a lot longer to reach a steady state.

32
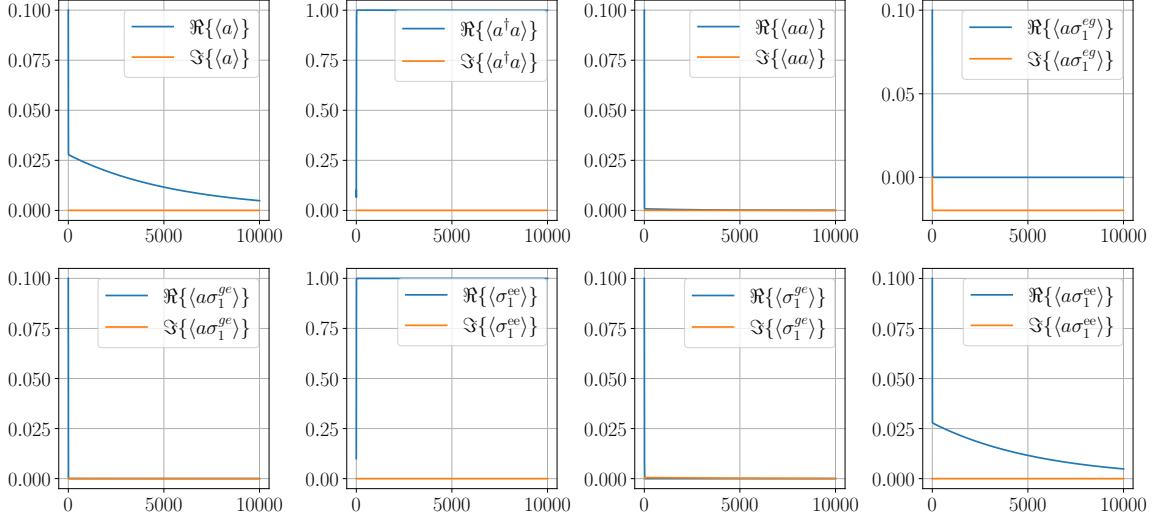
Figure 4.10.: *Time evolution of the expectation value of each operator for $N_{\text{Cl}} = 40$ clusters and a cluster size of $K = 250$. Blue depicts the real part, while orange shows the imaginary part. The phase dependent terms damp out to zero and only the phase invariant terms survive, as expected. The other parameters are $\nu = 0.5$, $\gamma = 10^{-8}$, $\Delta = 0$, $g = 0.005$, $\sigma_{\text{v}} = 0$, $\kappa = 1$.*
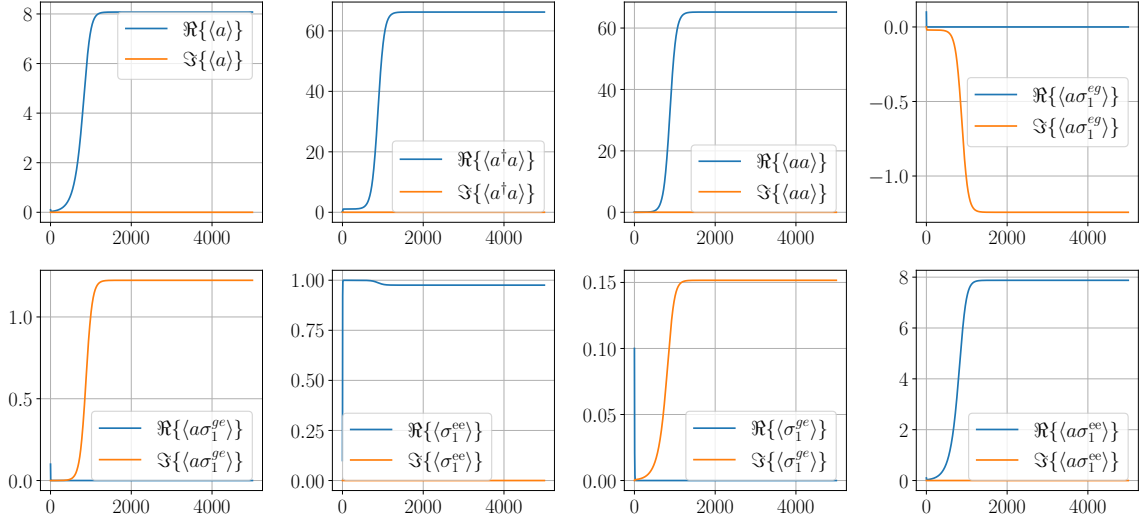
Figure 4.11.: *Time evolution of the expectation value of each operator for $N_{\text{Cl}} = 40$ clusters, but this time a cluster size of $K = 260$. Blue depicts the real part, while orange shows the imaginary part. Just increasing the cluster size from 250 to 260, the phase-dependent terms do not damp out anymore and contribute to the time evolution. The other parameters are the same as above.*

In order to gain more insight into how the parameters affect the state, we create phase plots in figures 4.12, 4.13, 4.14 and 4.15. The parameters in figures 4.12 and 4.13 are in the same region as the parameters in the plot before, where we had a look at when the phase terms damp out. In figure 4.12 we depict the absolute photon number in full mixed order, in figure 4.13 we depict the difference of full mixed order to reduced mixed order, and normalize with respect to the photon number in full mixed order. From this plot one can determine in which parameter regimes the reduced mixed order is a good approximation of the full mixed order. In 4.14 and 4.15 we do the same, but now for the parameter regime, that we have used to calculate all the previous results.

In figure 4.12 we see that we achieve large photon numbers for large atom numbers N, large interaction strength g and small σ_v. In figure 4.13 we see the normalized difference between full and reduced mixed order. In the blue region they are similar, while in the yellow region they differ a lot. Comparing to figure 4.12 we conclude that whenever the photon numbers are small, reduced and full mixed order agree with each other, with the exception of small pump rates ν (lower left graph). Moreover, we see that for large atom numbers and large interaction strength g (upper right corner of the plots in the left column) the difference begins to reduce. It is also important to note that the contour lines in the upper left plots (where we depict N_{Cl} vs. K) respectively show a typical $y = \frac{c}{x}$ behaviour, suggesting that the difference is not due to the artificial arrangement of the atoms into clusters.

In figure 4.14 and figure 4.15 we do the same, but now for a parameter region close to the parameters that we used to calculate most of the previous results. The absolute photon numbers for the new regime in figure 4.14 look qualitatively very similar to the result for the old parameter regime, but in general the photon numbers are much larger, as we now also have larger atom numbers. One difference regarding the pump strength ν appears: Increasing the pump strength leads to higher photon numbers, while in the old parameter regime an increased pump strength did not lead to more photons. The difference in full and reduced mixed order is depicted in figure 4.15. Qualitatively, it is similar to the plot for the old regime. However, as we now include much larger atom numbers in the new regime, we now look at a bigger range. We clearly see that for larger atom numbers the results begin to approach each other again in the green to blue regions in figure 4.15. In summary, it seems that reduced and full mixed order agree well for small photon numbers, and also for very large numbers of atoms. For our previously used parameters the reduced and full mixed order still disagree considerably and we should use full mixed order.
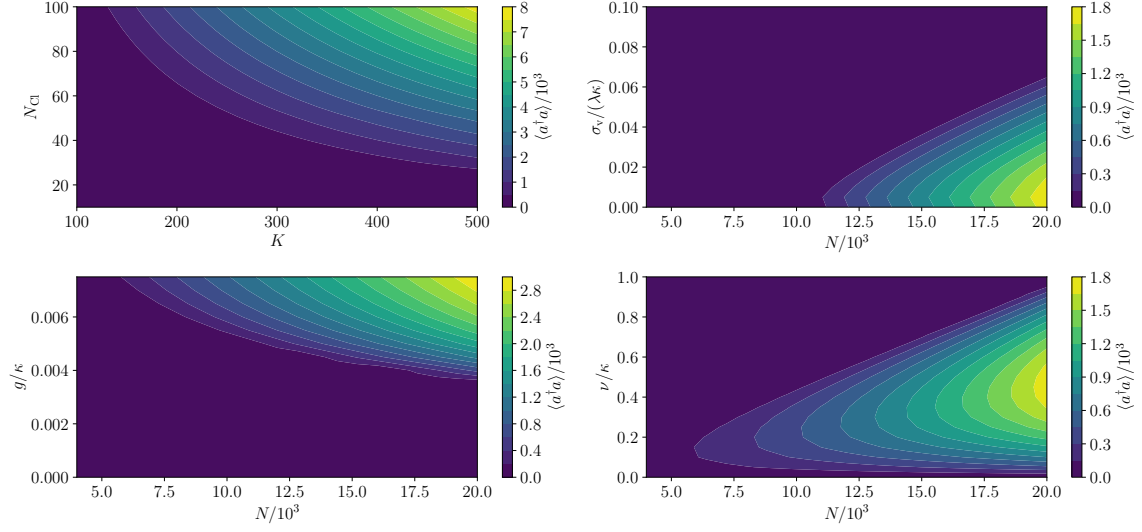
Figure 4.12.: *Photon numbers for different parameter regions.* We depict the photon number $\langle a^\dagger a \rangle$ in full mixed order. Blue indicates a small photon number, while a yellow colour means a large number of photons. The parameters (constant in each plot) are $N_{\mathrm{Cl}} = 40$, $\sigma_{\mathrm{v}} = 0$, $g = 0.005$ and $\nu = 0.5$.
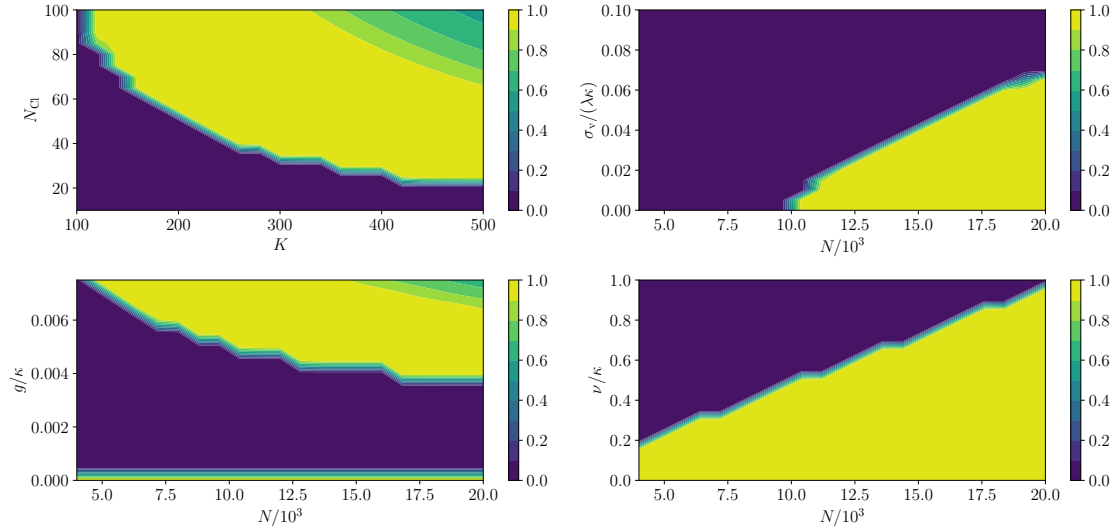
Figure 4.13.: *Difference of full and reduced mixed order.* We plot the absolute value of the difference in photon number between full mixed order and reduced mixed order. We normalize to the results in full mixed order. A large value (yellow) means that the phase terms do not cancel out and the results in full mixed order and reduced mixed order differ very much. On the contrary, in the blue region, they are close to each other. The parameters are the same as above.
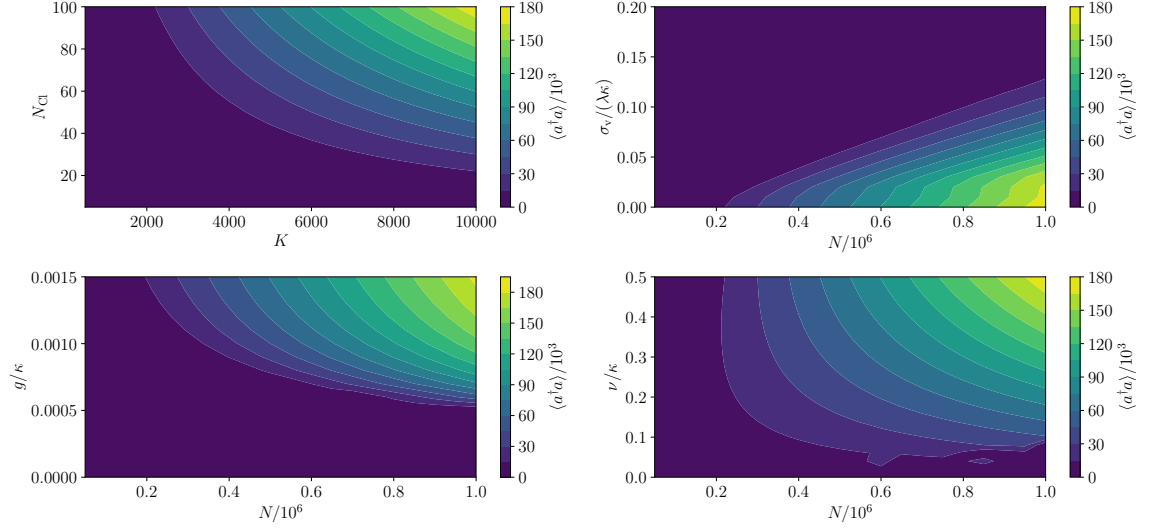
Figure 4.14.: *Photon numbers for different parameter regions.* We depict the photon number $\langle a^\dagger a \rangle$ in full mixed order. A blue colour indicates a small photon number, while a yellow colour means a large number of photons. The parameters (constant in each plot) are $N_{\mathrm{Cl}} = 100$, $\sigma_{\mathrm{v}} = 0$, $g = 0.00136$ and $\nu = 0.5$.
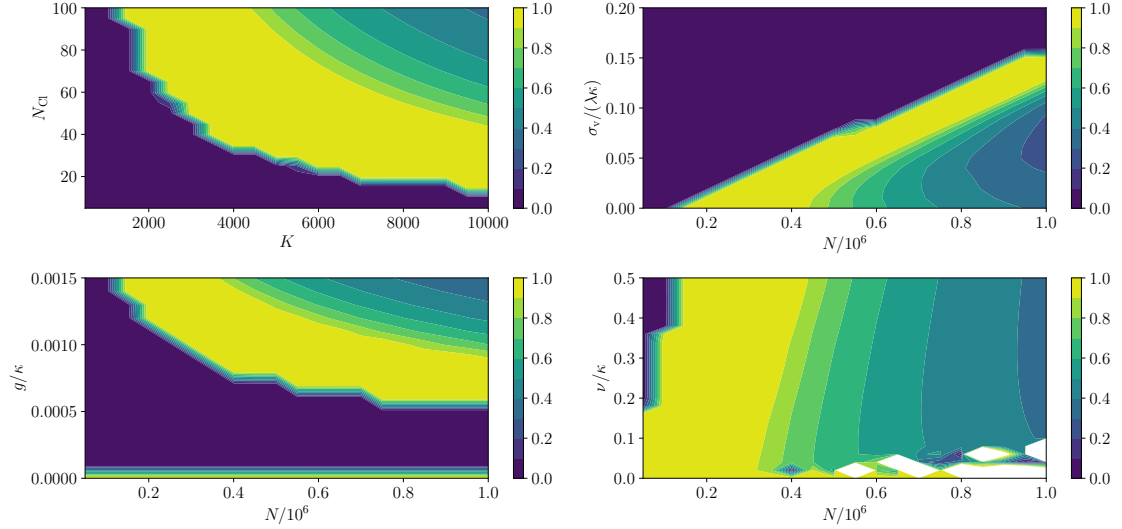
Figure 4.15.: *Difference of full and reduced mixed order.* We plot the absolute value of the difference in photon number between full mixed order and reduced mixed order. We normalize to the results in full mixed order. A large value (yellow) means, that the phase terms do not cancel out and the results in full mixed order and reduced mixed order differ very much. On the contrary, in the blue region, they are close to each other. In the white region the difference is so big, that it exceeds the colour bar. The parameters are the same as above.

4.4. Effects of a velocity filter to remove fast atoms

Another interesting idea is to consider a cutoff in the velocity distribution. By using such a velocity filter we get rid of the atoms with very high velocity, effectively creating a colder ensemble. This could be more beneficial than trying to narrow the velocity distribution by cooling, because cooling the atoms is experimentally difficult. In order to investigate this we again determine the average number of photons in quasi steady state by using multiple trajectories as in the previous sections. This time, however, we exclude the fast atoms from the dynamics. Figure 4.16 shows the results. To get a better comparison, the blue graph shows the previous result with no cut. The orange line represents the graph, when all atoms above 1.0 standard deviations are excluded from the dynamics, while the green graph does the same for a cut at 0.5 standard deviations. On the left-hand side, the absolute photon number is depicted. It is clearly visible that we end up with less photons in the cavity if we cut the distribution. This is not very suprising, as we also have less atoms contributing to the dynamics. On the right-hand side, the normalized photon numbers are shown, such that the maximum photon number for each cut (which occurs for very small σ_{v}) is set to one. Here, we see another feature: although we start with large photon numbers when using no cut, the photon numbers drop drastically with increasing σ_{v}, while the green line for a cut at 0.5 σ_{v} stays at a high level much longer with increasing σ_{v}. In summary, cutting the distribution leads to lower photon numbers, but the photon numbers for cut distributions are much less influenced by higher velocities (and therefore temperature) and one can tolerate a higher temperature, before the photon numbers drop drastically compared to the situation at zero temperature. However, it remains to be seen what such a cutoff will do to the linewidth of the laser light.
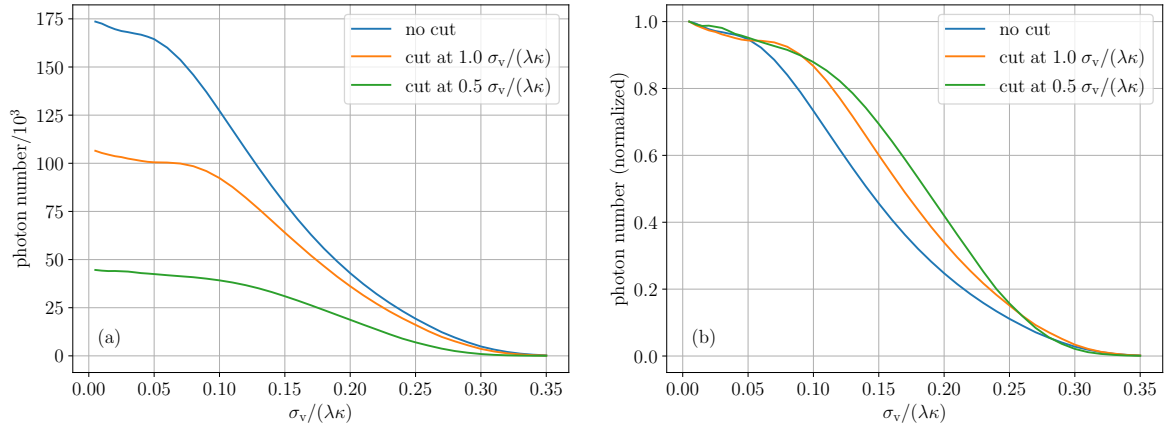
Figure 4.16.: *Photon numbers for different velocity cutoffs.* (a) Absolute photon number with different cutoffs. (b) Normalized to maximum photon number. Cutting the distribution yields smaller absolute photon numbers, but also leads to the photon numbers staying at a high level for increasing σ_{v}. We only depict the results in mean field, as the results in mixed order almost perfectly align. The parameters are $N_{\mathrm{Cl}} = 400$, $\nu = 0.5$, $\gamma = 10^{-8}$, $\Delta = 0$, $g = 0.00135$, $\kappa = 1$.

Chapter 5.

Conclusions and Outlook

We have numerically studied a laser system consisting of a single-mode cavity and up to 10^6 moving atoms. To be able to simulate such a high dimensional system we have used a cumulant expansion truncated at low orders. Another key approximation method was to group the atoms into clusters, such that the atoms within one cluster would be indistinguishable and could be considered identical. We have seen that such a grouping into clusters leads to valid results, even though we did not treat each atom individually.

The main novelty of this thesis is to include the motion of the atoms. We did this by assigning starting points and initial velocities to each atom while neglecting light forces and, thus, the path of each atom was known from the beginning of the simulation. We do not reach an actual steady-state, as the moving atoms will always result in fluctuations in the photon numbers. However, when choosing a sufficiently large number of clusters we reach a quasi steady state, at which the fluctuations oscillate around a certain value. This value can be determined by averaging over a lot of trajectories, and one unsurprisingly finds the highest photon numbers for no velocity at all. The photon numbers decrease with an increasing velocity of the atoms, until there are no photons inside the cavity anymore, which can be explained by the Doppler effect. Fixing the collective cooperativity parameter $\frac{g^2 N}{\kappa \gamma}$ to a certain value, we find that the photon numbers per atom are very similar and therefore they scale with $g^2 N^2$. When fixing all parameters except the number of atoms and the standard deviation of the velocity distribution, we see that a broader distribution can be compensated by a larger amount of atoms, such that we still end up with a lot of photons inside the cavity. A higher atom number does therefore not only lead to higher photon numbers in general, but also the photon numbers do not drop that fast with increasing σ_{v} (and therefore increasing temperature). Moreover, we see that the reduced mixed order can be used to approximate the full mixed order, but only in certain parameter regions, especially for low atom numbers. For our typical parameters we need to use the full mixed order. Furthermore, by using velocity filters for the atoms, one loses quite some photons, but now, increasing σ_{v} has much less of an impact on the photon numbers than for setups without a velocity filter. For a cut at 0.5 of the standard deviation of the distribution one can go to double the velocity compared to the full distribution, before a drastic drop in photon numbers appears.

The logical next task is to calculate the spectrum of the system as the most important property of a clock laser. As the system never reaches an exact steady-state, it is more subtle to obtain the correct spectrum compared to other systems. The approach of the so-called filter cavities might be useful here. Furthermore, it would be interesting to have a look at the system including light forces. Additionally, one could simulate the system in higher orders in the cumulant expansion, but one probably has to decrease the number of clusters to make it numerically feasible.

Appendices

Appendix A.

Dimensionless Equations for Numerical Simulations

In order to simulate a physical system, we need to solve the corresponding set of differential equations numerically, if they are to complicated to solve manually. For this purpose, we need to translate the set of differential equations with dimensions into numerical values only, as the computer only operates with mere numbers and does not care about dimensions or units. In principle, we can choose any consistent unit system, as the physical results do not change, regardless of the unit system in use. A straightforward choice would be the SI system, but, as this system was developed for everyday life rather than for quantum physics, we would have to deal with huge and very small numbers at the same time. While, in principle, this leads to the same result, it is very challenging for the computer to deal with such a big range of values, resulting in longer computational times. To find a good unit system, one usually identifies "typical" quantities that represent the scale on which the processes happen. In our case, we choose the planck constant $\hbar$ to be 1, this is very well known and widely used in quantum physics. Moreover, for the typical quantities of length and time (=inverse frequency) we choose the wavelength of the mode function λ and the mean lifetime of the photons emerging from the cavity $\frac{1}{\kappa}$, which is the inverse of the rate of decay κ. We choose a numerical value of 1 for these quantities, which means, that all lengths are given in terms of the period of the mode function and times are given in terms of the mean lifetime of a photon inside the cavity. To ensure consistency in the unit system, we see that by choosing the time scale we also have chosen the frequency scale to be κ. All frequencies are therefore measured in terms of the photon decay rate κ. In summary, we have for lengths s, times t and frequencies ω

- $t = \tilde{t} \cdot \frac{1}{\kappa}$

- $s = \tilde{s} \cdot \lambda$

- $\omega = \tilde{\omega} \cdot \kappa$.

The tilde indicates that the variable is just a numerical value. In order to get the actual value in another unit system $(s, t, \omega, ...)$, one has to multiply the numerical value

$(\tilde{s}, \tilde{t}, \tilde{\omega})$ in the result with the actual value of the "typical" quantities $(\lambda, \frac{1}{\kappa}, \kappa)$ in said unit system.

Moreover, in the following let us link the important quantity of temperature T to the related quantity of the standard deviation of the velocity distribution, σ_{v}. As we know, the temperature is related to the kinetic energy as

$$E = \frac{m \sum_i \langle v_i^2 \rangle}{2} = \frac{f}{2} \, k \, T, \tag{A.1}$$

where f is the number of spatial degrees of freedom ($f = 1$ in our case, as we are in 1D), k the Boltzmann constant and m the masses of the particles (assuming all particles have the same mass). To express $\sum_i \langle v_i^2 \rangle$ via the quantity σ_{v}, one has to calculate the second moment of a 1D Gaussian distribution. Well known substitutions lead to the result $\sum_i \langle v_i^2 \rangle = (\sigma_{\mathrm{v}})^2$. Altogether, we arrive at the following term expressing the temperature T via the standard deviation in the velocity distribution σ_{v},

$$T = \frac{m \cdot (\sigma_{\mathrm{v}})^2}{f \cdot k}. \tag{A.2}$$

Appendix B.

Program Example

The following programs are examples of what we have been using to perform the numerical simulations. The first program uses the julia package QuantumCumulants and derives the equations by itself. This has been mainly used to check the manually derived equations and to simulate the system in second order.

```julia
#import necessary libraries
using QuantumCumulants
using OrdinaryDiffEq
using ModelingToolkit
using PyPlot
using Random
using DelimitedFiles

M=1 #choose order of cumulant expansion
NCl=5 #Number of atom clusters

#define symbolic parameters
@cnumbers K Δ g κ Γ R ν t σv
v=[cnumbers(Symbol(:v, i))[1] for i=1:NCl]

#define atom trajectories
x0=[i/NCl for i=1:NCl]
xt=[x0[i]+v[i]*t for i=1:NCl]
phit=xt*2pi

#define Hilbert space
hc=FockSpace(:cavity)
ha_2l(i) = NLevelSpace(Symbol(:atom, i), 2)
ha_clust(i) = ClusterSpace(ha_2l(i), K, M)

ha = ⊗([ha_clust(i) for i=1:NCl]...)
h = hc ⊗ ha;
```

```julia
# operators
@qnumbers a::Destroy(h)
σ(i, j, k) = Transition(h, Symbol(:σ, k), i, j, k+1)

#define Hamiltonian
H = Δ*a'*a + sum([g*cos(phit[i])*(a'*sum(σ(1,2,i))+a*sum(σ(2,1,i))) for i=1:NCl])

#Lindblad terms for dissipative processes
J = [a; [σ(1,2,i) for i=1:NCl];[σ(2,1,i) for i=1:NCl];]
rates = [κ; [Γ for i=1:NCl]; [ν for i=1:NCl];];

# Derive equations
ops = [a] #for this operator(s) the equations will be derived
eqs = meanfield(ops,H,J; rates=rates, iv=t, order=M);

#custom filter function (only relevant for 2nd order)
φ(x::Average) = φ(x.arguments[1])
φ(::Destroy) = -1
φ(::Create) = 1
φ(x::QTerm) = sum(map(φ, x.args_nc))
φ(x::Transition) = x.i - x.j
phase_invariant(x) = iszero(φ(x))

#Complete equations starting with equation for ops
#eqs_c = complete(eqs; filter_func=phase_invariant) #use this for 2nd order
eqs_c = complete(eqs, multithread=true); #use this for mean field

#define ODE system, which can be solved numerically
sys = ODESystem(eqs_c);

#define function giving the solution, depending on parameters
function photnumbevo(T_end, K_, ν_, σv_, i, γ_, g_)

u0=[0.01 + 0.0*im for i=1:length(eqs_c)]
κ_ = 1
Δ_ = 0
Random.seed!(i) #allows us to have the same random distribution for the same i
v_=[randn()*σv for i=1:NCl]
ps=[K, Δ, g, κ, Γ, ν, σv, v...]
p0=[K_, Δ_, g_, κ_, γ_, ν_, σv_, v_...]
```

```julia
prob=ODEProblem(sys, u0, (0.0, T_end), ps.=>p0);
sol = solve(prob, Tsit5(), maxiters=1e7, saveat=0.1);
    return abs2.(sol[a])
    #return abs2.(sol[a])
end


#calculate a result
res=photnumbevo(400, 200000, 0.5, 0.0, 1, 10^(-8), 0.00136);


#plotting
tarr=collect(0.0:0.1:400)
plot(tarr, res)
```

In the second program, we make use of a standard Differential equations solver, but we have to write the equations down manually (in this example for mixed order). This program (or similar ones) were used for numerics.

```julia
#import necessary libraries
using DifferentialEquations
using PyPlot
using DelimitedFiles
using Statistics
using Random


#define function which returns solution to set of differential equations
function photnumbevo(T_end, K, NCl, ν, σv, i, γ, g)


#define fixed parameters
κ=1
Δ=0


function G(x)
    λ=1
    k=(2*pi)/λ
    return g*cos(k*x)
end


#define atom trajectories
x0=[j/NCl for j=1:NCl]
Random.seed!(i)
v0=[randn()*σv for j=1:NCl]
```

```
function cavityall(du, u, p, t)

xt=[x0[i]+t*v0[i] for i=1:NCl]
#abbreviations
aσparr=[G(x0[i]+t*v0[i])*u[i+3] for i=1:NCl]
aσp=sum(aσparr)

aσmarr=[G(x0[i]+t*v0[i])*u[NCl+i+3] for i=1:NCl]
aσm=sum(aσmarr)

σpσmarr=[G(x0[i]+t*v0[i])*u[2*NCl+i+3] for i=1:NCl]
σpσm=sum(σpσmarr)

σmarr=[G(x0[i]+t*v0[i])*u[3*NCl+i+3] for i=1:NCl]
σm=sum(σmarr)
pσm=[σm-σmarr[i] for i=1:NCl]



# write down manually derived equations in mixed order
# for mean field we need completely different equations
du[1]=-(κ/2-im*Δ)*u[1]  - im*K*σm #for <a>
du[2]= -(κ-2*im*Δ)*u[2] + im*K*(aσp - conj(aσp)) #for <a^†a>
du[3]=-(κ-2*im*Δ)*u[3] - 2*im*K*aσm #for <aa>

#use loop for each cluster
for i=4:(3+NCl) #eq for <aσ+>
du[i]=  -(κ/2+γ/2+ν/2-im*Δ)*u[i] + im*G(xt[i-3])*u[2] -im*G(xt[i-3])*u[i+2*NCl]+
        -2*im*G(xt[i-3])*(u[2]*u[i+2*NCl]+u[1]*conj(u[i+4*NCl])+
        +u[i+4*NCl]*conj(u[1])-2*u[1]*conj(u[1])*u[i+2*NCl]) +
        -im*K*conj(u[i+3*NCl])*pσm[i-3] +
        -im*G(xt[i-3])*(K-1)*conj(u[i+3*NCl])*u[i+3*NCl]-im*G(xt[i-3])*u[i+2*NCl]
end

for i=(4+NCl):(3+2*NCl) #eq for <aσ->
du[i]=  -(κ/2+γ/2+ν/2-im*Δ)*u[i]- im*G(xt[i-3-NCl])*u[3]+
        +2*im*G(xt[i-3-NCl])*(u[3]*u[i+NCl]+2*u[1]*u[i+3*NCl]-2*u[1]*u[1]*u[i+NCl]) +
        - im*K*u[i+2*NCl]*pσm[i-3-NCl]-im*G(xt[i-3-NCl])*(K-1)*u[i+2*NCl]*u[i+2*NCl]

end

for i=(4+2*NCl):(3+3*NCl) #eq for <σee>
du[i]=  - (γ+ν)*u[i] + ν+im*G(xt[i-3-2*NCl])*(conj(u[i-2*NCl]) - u[i-2*NCl])
```

47

```julia
end

for i=(4+3*NCl):(3+4*NCl) #eq for <σ->
du[i]=  -(γ+ν)/2*u[i]-im*G(xt[i-3-3*NCl])*u[1]+ 2*im*G(xt[i-3-3*NCl])*u[i+NCl]
end

for i=(4+4*NCl):(3+5*NCl)  #eq for <aσee>
du[i]=  -(γ+ν+κ/2-im*Δ)*u[i] + ν*u[1]- im*G(xt[i-3-4*NCl])*(u[3]*conj(u[i-NCl])+
        +2*u[1]*u[i-4*NCl]-2*u[1]*u[1]*conj(u[i-NCl])) +
        +im*G(xt[i-3-4*NCl])*(u[2]*u[i-NCl]+conj(u[i-4*NCl])*u[1]+
        +u[i-3*NCl]*conj(u[1])-2*conj(u[1])*u[1]*u[i-NCl]) +
        -im*K*u[i-2*NCl]*pσm[i-3-4*NCl]-im*G(xt[i-3-4*NCl])*(K-1)*u[i-2*NCl]*u[i-NCl]
end
end

# initial conditions
u0=[0.01+0.0*im for i=1:(3+5*NCl)]

tspan=(0.0, T_end)
prob=ODEProblem(cavityall, u0, tspan)
sol=solve(prob, saveat=0.1);

#pick solutions for interesting field operators
return [sol[1, :], sol[2, :], sol[3, :], sol[4, :], sol[2*NCl+2, :], sol[3*NCl+2, :]]
end

#define function calculating for different seeds and save the data in an array
function calcdata(T_end, K, NCl, ν, σv, g, samplesize)

    #save data in txt file with parameters in name
    open("inhom/qmixed_Tend$T_end.K$K.NCl$NCl.nu$ν.sv$σv.g$g.txt", "w") do io
        ini=1
        for j=(ini):(ini+samplesize-1)
        writedlm(io, [abs.(photnumbevo(T_end, K, NCl, ν, σv, j, 10^(-8), g)[2])])
        end
    end
end

tableK=[2500, 2000, 1500, 1000, 500]
scanv1=collect(0.0:0.01:0.1)
scanv2=collect(0.12:0.02:0.7)
scanv=0.5*vcat(scanv1, scanv2);
```

```julia
using ProgressMeter
prog=Progress(length(tableK)*length(scanv))

#calculate for all parameters using a loop
samplesize=50;
for i in 1:length(tableK)
Threads.@threads for j in 1:length(scanv)
            calcdata(400, tableK[i], 400, 0.5, scanv[j],0.00136, samplesize)
            next!(prog)
        end
end

#reads out data from txt file
function readout_te(T_end, K, NCl, ν, σv, g)
    yprob=readdlm("qmixed_Tend$T_end.K$K.NCl$NCl.nu$ν.sv$σv.g$g.txt");
    te=sum(yprob, dims=1)
    return transpose(te)/size(yprob, 1)
    #averaging over all trajectories with different random distributions
end

function readout_av(T_end, K, NCl, ν, σv, g)
    yprob=readout_te(T_end, K, NCl, ν, σv, g)
    #average over each trajectory
    sum=0;
    start=2000; #at this time the quasi-steady-state is achieved
    size=length(yprob)-start+1;
    for i=start:length(yprob)
        sum+=yprob[i]
    end
    return sum/size
end

#reads out average quasi-steady state values and plots them
function readout_graph(T_end, K, NCl, ν, g)
    graph=zeros(length(scanv))
    graph=readout_av.(T_end, K, NCl, ν, scanv, g)
 plot(scanv, graph)
return graph
end
```

Bibliography

[1] D. Meiser, Jun Ye, D. R. Carlson, and M. J. Holland. Prospects for a millihertz-linewidth laser. *Phys. Rev. Lett.*, 102:163601, 2009.

[2] R. H. Dicke. Coherence in spontaneous radiation processes. *Phys. Rev.*, 93:99–110, Jan 1954.

[3] M. Gross and S. Haroche. Superradiance: An essay on the theory of collective spontaneous emission. *Physics Reports*, 93(5):301–396, 1982.

[4] Fritz Haake, Mikhail I. Kolobov, Claude Fabre, Elisabeth Giacobino, and Serge Reynaud. Superradiant laser. *Phys. Rev. Lett.*, 71:995–998, Aug 1993.

[5] Justin Bohnet, Zilong Chen, Joshua Weiner, Dominic Meiser, Murray Holland, and James Thompson. A steady-state superradiant laser with less than one intracavity photon. *Nature*, 484:78–81, 04 2012.

[6] Haonan Liu, Simon B. Jäger, Xianquan Yu, Steven Touzard, Athreya Shankar, Murray J. Holland, and Travis L. Nicholson. Rugged mhz-linewidth superradiant laser driven by a hot atomic beam. *Phys. Rev. Lett.*, 125:253602, Dec 2020.

[7] Kamanasish Debnath, Yuan Zhang, and Klaus Mølmer. Lasing in the superradiant crossover regime. *Physical Review A*, 98(6), Dec 2018.

[8] Mikkel Tang, Stefan A. Schäffer, Asbjørn A. Jørgensen, Martin R. Henriksen, Bjarke T. R. Christensen, Jörg H. Müller, and Jan W. Thomsen. Cavity-immune features in the spectra of superradiant crossover laser pulses, 2021.

[9] Miguel Orszag. *Quantum Optics*. Springer, 2008.

[10] Christoph Gerry and Peter Knigt. *Introductory Quantum Optics*. Cambridge University Press, 2004.

[11] Crisphin Gardiner and Peter Zoller. *The Quantum World of ultra-cold Atoms and Light, Book 1: Foundations of Quantum Optics*, volume 2. Imperial College Press, 2014.

[12] Kathrin Sandner. *Cavity quantum electrodynamics with ultracold atoms and superconducting resonators*. PhD thesis, Universität Innsbruck, 9 2012.

[13] Christoph Hotter. Superradiant cooling, trapping and lasing of dipole-interacting clock atoms. Master's thesis, Universität Innsbruck, 12 2018.

[14] Ryogo Kubo. Generalized cumulant expansion method. *Journal of the Physical Society of Japan*, 17(7):1100–1120, 1962.

[15] N.G. Van Kampen. A cumulant expansion for stochastic linear differential equations. i. *Physica*, 74(2):215–238, 1974.

[16] N.G. Van Kampen. A cumulant expansion for stochastic linear differential equations. ii. *Physica*, 74(2):239–247, 1974.

[17] David Plankensteiner, Christoph Hotter, and Helmut Ritsch. Quantumcumulants.jl: A julia framework for generalized mean-field equations in open quantum systems, 2021.